Biology Direct

RESEARCH

Open Access

Deciphering MOSPD1's impact on breast cancer progression and therapeutic response

Yiling Jiang[1†], Hailong Li[2†], Sixuan Wu[1], Baohong Jiang[3], Lijun Zeng[1], Yuanbin Tang[1], Lunqi Luo[1], Lianjie Ouyang[1], Wei Du[2] and Yuehua Li[1*]

Abstract

Background Motile Sperm Domain-Containing Protein 1 (MOSPD1) has been implicated in breast cancer (BC) pathophysiology, but its exact role remains unclear. This study aimed to assess MOSPD1 expression levels in BC versus normal tissues and investigate its diagnostic potential.

Methods MOSPD1 expression was analyzed in BC and normal tissues, with Receiver Operating Characteristic analysis for diagnostic evaluation. Validation was performed using immunohistochemistry. Functional studies included tumor growth assays, MOSPD1 suppression and overexpression experiments, and testing BC cell responses to anti-PD-L1 therapy.

Results MOSPD1 expression was significantly higher in BC samples than normal tissues, correlating with poor clinical outcomes in BC patients. MOSPD1 suppression inhibited tumor growth, while overexpression accelerated it. Silencing MOSPD1 enhanced BC cell sensitivity to anti-PD-L1 therapy and decreased Th2 cell activity. In vivo experiments supported these findings, showing the impact of MOSPD1 on tumor growth and response to therapy.

Conclusions Elevated MOSPD1 levels in BC suggest its potential as a biomarker for adverse outcomes. Targeting MOSPD1, particularly with anti-PD-L1 therapy, may effectively inhibit BC tumor growth and modulate immune responses. This study emphasizes the significance of MOSPD1 in BC pathophysiology and highlights its promise as a therapeutic target.

Keywords MOSPD1, Breast cancer, Th2 cells, PD-L1 inhibitors, Tumor microenvironment, Immune cell infiltration

Introduction

Breast cancer (BC) is the most common malignant tumor in women worldwide, with many new cases and deaths reported yearly [1]. Global distribution of BC indicates a higher prevalence in industrialized nations, which may be closely linked to factors such as lifestyle, reproductive patterns, dietary habits, and genetic background [2]. Epidemiological characteristics of BC reveal significant variations in incidence rates among different regions and ethnicities, potentially associated with genetic, environmental, and lifestyle factors [3, 4]. Although there have been significant advancements in the early diagnosis and treatment methods of BC over the past few decades,

†Yiling Jiang and Hailong Li are regarded as co-first authors.

*Correspondence:
Yuehua Li
liyuehua2020@stu.usc.edu.cn
[1]Department of Oncology, The First Affiliated Hospital, Hengyang Medical School, University of South China, No. 69 Chuanshan Road, Hengyang, Hunan Province 421001, People's Republic of China
[2]Department of pathology, Changde Hospital, Xiangya School of Medicine, Central South University (The first people's hospital of Changde city), Changde City 415000, Hunan, People's Republic of China
[3]Department of Pharmacy, The First Affiliated Hospital, Hengyang Medical School, University of South China, No. 69 Chuanshan Road, Hengyang 421001, Hunan, People's Republic of China

many patients still face unfavorable prognoses due to disease recurrence or metastasis [5, 6]. The occurrence and progression of breast cancer is a complex process involving interactions among various cells and molecules [7, 8], in which factors such as hormone receptor status, HER2 expression, and gene mutations play critical roles in breast cancer development [9].

The onset and progression of BC are complex processes involving interactions between various cells and molecules [7, 8]. Factors such as hormone receptor status, HER2 expression, and gene mutations play critical roles in the development of BC [10]. The nuanced interplay of these factors dictates the aggressive behavior of the tumor and its response to treatment, underscoring the need for targeted molecular interventions.

In recent years, the role of immune cell infiltration in BC has gained widespread attention, as they play a critical regulatory role in the tumor microenvironment, affecting BC growth, metastasis, and treatment responses [11, 12]. The interaction between the immune system and tumor cells is currently a focal point in cancer research. Studies indicate that various immune cells in the tumor microenvironment can either promote or inhibit the development of tumors through different mechanisms [13, 14]. The dynamic regulation of these immune cells can potentially be manipulated to enhance therapeutic efficacy and patient survival.

Among the immune regulatory factors, the major sperm protein domain-containing 1 (MOSPD1) has emerged as a novel research focus, with its expression and functions in various tumors gradually being elucidated [15]. MOSPD1 is a member of the gene family that includes MOSPD2 and MOSPD3, characterized by a sperm protein domain and two transmembrane domains [16]. Although there are currently few literature reports on the role of MOSPD1 in tumors, increasing evidence suggests that MOSPD1 may play essential roles in various tumors, especially in terms of immune cell infiltration and immune responses [17, 18]. The Cancer Genome Atlas (TCGA) analysis revealed a significant upregulation of MOSPD1 in BC. Studies on prostate cancer have also indicated an elevated expression of MOSPD1 in tumor cells regulated by the β-catenin/TCF7L2 complex. Given this background, investigating MOSPD1 could reveal novel approaches to modulate the immune landscape of BC, offering avenues for developing immune-based therapies.

Immune cell infiltration is a critical factor in the tumor microenvironment, significantly impacting tumor growth, metastasis, and treatment responses [19]. Research has found that specific immune cells, such as Th2 cells, might have promotive roles in tumors, while other immune cells may have inhibitory effects [20, 21]. Furthermore, immune cell infiltration is associated with the treatment response to immune checkpoint inhibitors like anti-PD-L1 [22], providing new opportunities for targeted BC treatment.

As BC treatment enters a new era of personalized medicine, understanding how molecules like MOSPD1 regulate immune responses in the tumor microenvironment is crucial for developing more effective treatment strategies. These novel treatment approaches may involve targeted therapies against specific immune cell subtypes to optimize tumor response to existing drugs and reduce the risk of recurrence. Targeting MOSPD1 could, therefore, personalize and enhance the immunotherapeutic approaches, tailoring them to the unique tumor microenvironment of each patient. By delving into MOSPD1 and related pathways, patients can be offered precise treatment options, ultimately improving prognosis and quality of life.

Given the background above, this study aims to explore the role of MOSPD1 in BC, especially its regulation of immune cell infiltration, Th2 cell activity, and drug sensitivity to anti-PD-L1. Through this research, we hope to provide new molecular markers and potential therapeutic targets for BC's early diagnosis, treatment, and prognosis assessment, deepening the understanding of the molecular mechanisms of BC onset and progression and offering better clinical treatment options.

Materials and methods

RNA sequencing data Collection and Processing

We selected gene expression data (HTSeq-FPKM) of 1083 breast cancer (BC) cases from The Cancer Genome Atlas (TCGA) database for the study and further filtered data with corresponding clinical information for further analysis (Table 1). The HTSeq-FPKM data were transformed into Transcripts Per Million (TPM) to enhance data comparability. Subsequently, patient data were divided into high and low-expression groups based on the median expression level of MOSPD1. As the data used are from public databases and have been de-identified, no further ethical approval or informed consent was required for this study.

Tissue microarray preparation and immunohistochemistry

To delve deeper into MOSPD1 expression in BC, we extracted tumorous tissues and their corresponding paratumorous tissues from 44 BC patients and prepared them into tissue microarrays. After paraffin embedding these tissue samples, they were stained for immunohistochemistry using MOSPD1 antibody at a 1:100 concentration, subsequently enhanced with horseradish peroxidase-linked secondary antibody (Dako Cyomation, Carpinteria, CA, USA). Staining results were independently assessed by two experienced pathologists, with scoring criteria as 0 (negative), 1 (weakly positive),

Table 1 Baseline data of 1,083 breast cancer (BC) cases selected from the TCGA database

Characteristic	Low expression of MOSPD1	High expression of MOSPD1	*P* value
n	541	542	
T stage, n (%)			0.086
T1	149 (13.8%)	128 (11.9%)	
T2	299 (27.7%)	330 (30.6%)	
T3	78 (7.2%)	61 (5.6%)	
T4	14 (1.3%)	21 (1.9%)	
N stage, n (%)			0.045
N0	280 (26.3%)	234 (22%)	
N1	165 (15.5%)	193 (18.1%)	
N2	51 (4.8%)	65 (6.1%)	
N3	37 (3.5%)	39 (3.7%)	
M stage, n (%)			0.325
M0	439 (47.6%)	463 (50.2%)	
M1	7 (0.8%)	13 (1.4%)	
Pathologic stage, n (%)			0.053
Stage I	106 (10%)	75 (7.1%)	
Stage II	302 (28.5%)	317 (29.9%)	
Stage III	119 (11.2%)	123 (11.6%)	
Stage IV	6 (0.6%)	12 (1.1%)	
Race, n (%)			0.092
Asian	26 (2.6%)	34 (3.4%)	
Black or African American	104 (10.5%)	77 (7.7%)	
White	376 (37.8%)	377 (37.9%)	
Age, n (%)			0.649
<=60	296 (27.3%)	305 (28.2%)	
>60	245 (22.6%)	237 (21.9%)	
Histological type, n (%)			< 0.001
Infiltrating Ductal Carcinoma	338 (34.6%)	434 (44.4%)	
Infiltrating Lobular Carcinoma	141 (14.4%)	64 (6.6%)	
PR status, n (%)			0.194
Negative	157 (15.2%)	185 (17.9%)	
Indeterminate	2 (0.2%)	2 (0.2%)	
Positive	359 (34.7%)	329 (31.8%)	
ER status, n (%)			0.008
Negative	101 (9.8%)	139 (13.4%)	
Indeterminate	1 (0.1%)	1 (0.1%)	
Positive	416 (40.2%)	377 (36.4%)	
HER2 status, n (%)			0.346
Negative	281 (38.7%)	277 (38.1%)	
Indeterminate	8 (1.1%)	4 (0.6%)	
Positive	73 (10%)	84 (11.6%)	
PAM50, n (%)			< 0.001
Normal	28 (2.6%)	12 (1.1%)	
LumA	310 (28.6%)	252 (23.3%)	
LumB	85 (7.8%)	119 (11%)	
Her2	39 (3.6%)	43 (4%)	
Basal	79 (7.3%)	116 (10.7%)	
Menopause status, n (%)			0.940
Pre	118 (12.1%)	111 (11.4%)	
Peri	20 (2.1%)	20 (2.1%)	
Post	353 (36.3%)	350 (36%)	
Anatomic neoplasm subdivisions, n (%)			0.236
Left	271 (25%)	292 (27%)	

Table 1 (continued)

Characteristic	Low expression of MOSPD1	High expression of MOSPD1	*P* value
Right	270 (24.9%)	250 (23.1%)	
radiation_therapy, n (%)			0.064
No	208 (21.1%)	226 (22.9%)	
Yes	299 (30.3%)	254 (25.7%)	
Age, meidan (IQR)	59 (48, 67)	58 (49, 67)	0.876

2 (moderately positive), and 3 (strongly positive). Additionally, scores of 1, 0–10%; 2, 11–50%; 3, 51–80%; 4, 81–100% were given based on the percentage of positively stained cells. Adding these two scores, results greater than or equal to 4 were defined as high expression of MOSPD1, and those less than 4 were considered low expression.

Identification of differentially expressed genes (DEGs) and protein-protein interaction

To further study genes co-expressed with MOSPD1 and their role in the protein-protein interaction network, we utilized the String analysis tool to predict potential protein-protein interaction relationships. In this analysis, interactions with a composite score greater than 0.4 were considered statistically significant. Furthermore, we compared the gene expression profiles of the high MOSPD1 expression group with the low MOSPD1 expression group to identify DEGs. Analysis was performed using the DESeq2 (3.8) package in R, with statistical testing conducted using the Wilcoxon rank-sum test. In this analysis, we set |log2FC|>1 and an adjusted P-value less than 0.05 as the threshold criteria for determining DEGs.

Gene set enrichment analysis (GSEA)

To uncover functional differences between high and low expression states of MOSPD1 in BC, we employed Gene Set Enrichment Analysis (GSEA). The core idea of the GSEA method is to determine if there's a statistically significant functional difference between two biological states (e.g., high and low expression of MOSPD1) by comparing against a predefined set of genes. In this analysis, calculations were performed using the ClusterProfiler package in R, ensuring that each analysis was repeated 1000 times to ensure result stability. After calculations, functions or pathways with an adjusted P-value less than 0.05 and a False Discovery Rate (FDR) less than 0.25 exhibited significant enrichment differences.

Single sample GSEA (ssGSEA) immune infiltration analysis

To delve deeper into BC samples' immune cell infiltration characteristics, we used the single-sample GSEA (ssGSEA) method and the GSVA package in R for analysis. This method evaluated 24 different types of immune cells, covering everything from mast cells, neutrophils, and Natural Killer (NK) cells to cytotoxic cells. This evaluation was based on signature gene sets specific to each cell, providing relative enrichment scores for each type of immune cell in each BC sample. Furthermore, we employed the Spearman correlation coefficient analysis to explore the association between BC and each immune cell subset. Lastly, to compare immune cell infiltration differences between the high and low MOSPD1 expression groups, we utilized the Wilcoxon rank-sum test for evaluation.

Assessment of stromal score, immune score, and estimation score

To evaluate the stromal score, immune score and estimation score in BC samples, we calculated each sample using the ESTIMATE algorithm. After obtaining these scores, we utilized R's "limma" and "estimate" packages to explore the correlation between MOSPD1 expression and stromal and immune scores.

Correlation analysis of MOSPD1 with immune checkpoint genes

We conducted a co-expression analysis to explore the potential relationship between MOSPD1 and immune checkpoint genes further. Using the "limma," "reshape2," and "RColorBrewer" packages in R, we systematically compared the expression of MOSPD1 with a myriad of immune checkpoint genes.

Construction and evaluation of nomogram

The results of multivariate analysis were utilized to construct a nomogram to individually predict 1, 3, and 5-year survival probabilities. We used the RMS R package to generate the nomogram and calibrated the calibration plot with clinical features significantly correlated with MOSPD1. The most common methods to evaluate model performance are calibration and discrimination. In this study, we calculated the calibration curve by mapping the nomogram-predicted probabilities with the observed rates, where a 45-degree line represents the best prediction. To determine the discriminative ability of the nomogram, the concordance index (c-index) was computed using a bootstrap method with 1000 resamples. Additionally, we employed the c-index and ROC analysis to compare the predictive accuracy of the nomogram with individual prognostic factors. All two-sided tests were set at a statistical significance level of 0.05.

Cell culture and transfection

The human BC cell lines MCF-7 (HTB-22, ATCC) and T47D (HTB-133, ATCC) provided by ATCC were utilized. The cells were cultured in RPMI 1640 medium (11875093, Gibco) supplemented with 1% penicillin-streptomycin (Invitrogen) and 10% fetal bovine serum (A5669701, Gibco) to maintain optimal growth conditions at 37 °C in a 5% CO_2 cell culture incubator. Upon reaching 80% confluency, cells were passaged by digestion with 0.25% trypsin/EDTA (25200072).

Transfection experiments were conducted to investigate the role of MOSPD1 in MCF-7 and T47D cells. MCF-7 and T47D cells were divided into six groups: (1) oe-NC group; (2) oe-MOSPD1 group; (3) sh-NC group; (4) sh-MOSPD1 group; (5) sh-MOSPD1 + oe-NC group; (6) sh-MOSPD1 + oe-MOSPD1 group. Transfections were performed when the cell confluency reached 50% using Lipofectamine 3000 transfection reagent (L3000075, Thermo Fisher Scientific) following the manufacturer's instructions. Expression and knockdown vectors of MOSPD1 were obtained from Shanghai Hanheng Biotechnology Co., Ltd. After 48 h of transfection; puromycin selection was carried out to ensure a successful introduction of the target gene into the cells. The efficiency of MOSPD1 expression or knockdown was verified by immunohistochemistry.

Construction of Nude Mouse Xenograft Model

6-8-week-old female NOD/ShiLtJGpt-Prkdcem26Cd52Il2rgem26Cd22/Gpt (huHSC-NCG) mice were procured from Jiangsu GemPharmatech Biotech Co., Ltd. These mouse model, which reconstructs the human immune system, was generated by intravenously injecting highly glycosylated type I transmembrane glycoprotein (CD34) + hematopoietic stem cells (HSCs) isolated from human umbilical cord blood into NCG mice. The mice were accommodated in a specialized SPF-grade animal facility, maintaining humidity at 60-65% and a temperature range of 22–25 °C. Continuous monitoring of the mice's health status was conducted after one week of acclimatization.

Unless otherwise specified, each experimental group involved 6 mice. Tumor transplantation models were established in the mammary fat pads of the mice using MCF-7 and T47D cell lines. The transfected cell lines were categorized into four groups: oe-NC group (transfected with an empty vector), oe-MOSPD1 group (transfected with a MOSPD1 overexpression vector), sh-NC group (transfected with an shRNA control vector), and sh-MOSPD1 group (transfected with an shRNA targeting MOSPD1). Further investigation into the interaction between MOSPD1 and PD-L1 led to the mice being subdivided into eight additional groups: sh-NC group, sh-MOSPD1 group, sh-NC + anti-PD-L1 group, sh-MOSPD1 + anti-PD-L1 group, oe-MOSPD1 group, oe-NC + anti-PD-L1 group, and oe-MOSPD1 + anti-PD-L1 group. The mice were administered intraperitoneal injections of 200 μg of control IgG (ab31380, Abcam; https://www.abcam.cn/) or 200 μg of anti-PD-L1 (orb622009, Biorbyt; https://www.biorbyt.com/) every three days. Regular measurement and recording of tumor volumes for each mouse were carried out throughout the experiment. Upon reaching an approximate tumor size of 500 mm^3, tumor tissues were harvested for subsequent analyses and experiments.

Immunohistochemistry

Tissue samples were fixed with 4% paraformaldehyde for 12 h, followed by embedding in paraffin and sectioning at a thickness of 3 μm. Deparaffinization was done using xylene, followed by hydration in a gradient of alcohol solutions (anhydrous ethanol, 95% ethanol, 75% ethanol for 3 min each). The sections were then subjected to antigen retrieval by boiling in 0.01 M citrate buffer for 15–20 min. Subsequent steps included blocking endogenous peroxidase activity by incubating in 3% H_2O_2 at room temperature for 30 min and blocking nonspecific binding sites with goat serum blocking solution for 20 min at room temperature. After adding primary antibodies (Ki-67, 1/100 dilution from ab15580, Abcam; MOSPD1, 1/500 dilution from HPA031158, Sigma) and incubating at room temperature for 1 h, the sections were washed with PBS. Subsequently, a secondary antibody (goat anti-rabbit IgG, 1/100 dilution from ab6721, Abcam) was added and incubated at 37 ℃ for 20 min, followed by PBS washes. The sections were then incubated with streptavidin peroxidase (SP) at 37 ℃ for 30 min, washed with PBS, and subjected to DAB staining (ST033, Guangzhou Weijia Technology Co., LTD) for 5–10 min, followed by a 10-minute water rinse to stop the reaction. Counterstaining was performed using hematoxylin for 2 min, followed by differentiation in acid alcohol, a 10-minute water rinse, dehydration in alcohol gradients, clearing in xylene, and mounting in neutral resin. Finally, the sections were observed and analyzed under a bright-field microscope (BX63, Olympus). Five random high-power fields per slide were chosen for observation, and the average optical density of the images was analyzed using Image-Pro Plus 6.0 software.

CCK-8 assay

The CCK-8 kit (WH1199, Shanghai Wellbio Biotechnology Co., Ltd., Shanghai, China, http://www.biotechwell.com/) was used to detect cell proliferation. Logarithmically growing cells were collected and adjusted to a concentration of 5×10^4 cells/mL in DMEM containing 10% FBS. The cells were then seeded into a 96-well culture plate at 100 μL per well and incubated for 24 h, 48 h,

and 72 h. The supernatant was quickly discarded, and 10 μL of CCK-8 solution was added to each well. After 2 h of incubation at 37 °C, the absorbance (A) was measured using a Multiskan FC microplate reader (51119080, Thermo Fisher Scientific, USA, https://www.thermofisher.cn/cn/zh/home.html) at a wavelength of 450 nm. The proliferation rate (%) was calculated as [(A_control - A_experimental)/A_control] × 100%. Three parallel wells were set for each group, and the average value was taken. The experiment was repeated three times.

Flow cytometry

Tumor tissue-derived single cells were collected, minced, and then digested at 37 ℃ for 1 h with 5 ml of 2 mg/ml collagenase (17018029, Sigma). Subsequently, cells were filtered through a 70 μm mesh, and red blood cell lysis was carried out by suspending the cell pellet in lysis buffer (C3702, Beyotime) for 5 min, followed by centrifugation to collect the cell pellet. The cells were resuspended in 0.5 ml of fixation buffer (420801, Biolegend) and fixed at room temperature for 20 min. After fixation, cells were washed twice with 1×PBS containing 2% BSA to permeabilize the cells before suspending them in an intracellular staining permeabilization buffer (421002, Biolegend). The cells were then stained with anti-CD3-PE (1:100, 12-0031-82, Thermo Fisher), anti-CD4-APC (1:100, MHCD0427, Thermo Fisher), and anti-IL-4-Alexa Fluor 488 (1:100, 53-7041-82, Thermo Fisher) antibodies. Incubation with the respective antibodies was done at room temperature for 30 min, followed by washing the cells with 1×PBS containing 2% BSA and analysis using a flow cytometer. Initially, cells positive for CD3 were gated, and subsequently, the proportion of CD4 and IL-4 double-positive cells within the CD3-positive cell population was analyzed [23].

TUNEL staining

Mouse tumor tissue was fixed in 4% paraformaldehyde for 15 min, followed by three washes with PBS and permeabilization in 0.1% Triton-X 100 in PBS for 3 min. Subsequently, BC tissue cells were stained using the TUNEL assay kit (C1091, Beyotime, China). Biotin labeling solution (50 μl) was added to the samples and incubated at 37 ℃ in the dark for 60 min, followed by three PBS washes. Next, 0.3 ml of the labeling reaction termination solution was added with subsequent PBS washes. Samples were treated with 50 μl of Streptavidin-HRP working solution at room temperature for 30 min, followed by three PBS washes. DAB chromogen solution (0.5 ml) was added and incubated at room temperature for 5 min, followed by three PBS washes. Counterstaining was performed using DAPI (10 μg/ml, C1025, Beyotime) for 10 min. Images from each group were observed using a confocal microscope (FV1000, Olympus) and analyzed for the percentage of apoptotic cells using Image-Pro Plus 6.0 software.

Table 2 RT-qPCR primer sequences

Gene	Primer sequence
Il-4	F 5′-CCGTAACAGACATCTTTGCTGCC-3′
	R 5′-GAGTGTCCTTCTCATGGTGGCT-3′
Il-5	F 5′-GGAATAGGCACACTGGAGAGTC-3′
	R 5′-CTCTCCGTCTTTCTTCTCCACAC-3′
Il-13	F 5′- TTGCACAGACCAAGGCCC-3′
	R 5′- TGGGTCCTGTAGATGGCATTGC – 3′
Gapdh	F 5′-CATCACTGCCACCCAGAAGACTG-3′
	R 5′-ATGCCAGTGAGCTTCCCGTTCAG-3′

Note: F, forward; R, reverse

RT-qPCR

Tumor tissue was lysed using the Trizol reagent kit (Invitrogen, Thermo Fisher) to extract total RNA. The quality and concentration of RNA were assessed using ultraviolet-visible spectrophotometry (ND-8000-GL, Thermo Fisher). For mRNA expression analysis, real-time quantitative reverse transcription-polymerase chain reaction (RT-qPCR) was performed using the One Step TB Green® PrimeScript™ RT-PCR Kit II (RR086A, TaKaRa) on the LightCycler 480 system (Roche Diagnostics, Pleasanton, CA, USA). GAPDH was used as the internal control. Primers for amplification were designed and provided by Shanghai General Biological Technology Co., Ltd. The primer sequences are listed in Table 2. The $2^{-\Delta\Delta Ct}$ method was used to determine the fold change in target gene expression between the experimental and control groups, calculated as follows: ΔΔCT = ΔCt experimental group - ΔCt control group, where ΔCt = target gene Ct - internal control gene Ct.

Statistical analysis

This study employed descriptive statistics to describe and summarize the data, with continuous variable results expressed as mean ± standard deviation and categorical variables as frequencies and percentages. The Wilcoxon rank-sum test was used to compare differences between two independent samples, and the ROC curve and AUC were employed to assess the diagnostic capability of MOSPD1 as a binary classifier. The relationship between MOSPD1 expression, clinical pathological features, and prognosis in BC patients was evaluated using Cox regression analysis and Kaplan-Meier survival analysis. Functional enrichment analysis was used to determine the hallmark pathways associated with high and low expression of MOSPD1. Based on the data distribution, the Pearson or Spearman correlation analysis assessed the correlation between MOSPD1 and other variables. The t-test or ANOVA was used to compare the mean differences of continuous variables between two or multiple

groups, while the chi-square test was utilized to assess the independence or association between categorical variables. All statistical analyses were conducted in SPSS version 26.0 (IBM, Armonk, NY) or R version 4.0.3 (R Foundation for Statistical Computing, Vienna, Austria), with a P-value of less than 0.05 considered statistically significant.

Results

Elevated expression of MOSPD1 in various tumor types and its diagnostic potential

Recent advancements in genomics have highlighted the potential of molecular markers in cancer diagnosis. Among these, MOSPD1 has emerged as a candidate gene of significant interest. In this section, we used TCGA data to explore the expression levels of MOSPD1 across different tumor types and assessed its potential as a diagnostic marker.

According to TCGA datasets, MOSPD1 exhibited significant overexpression in 19 out of 33 tumor types. Notably, this included BC, hepatocellular carcinoma (LIHC), cholangiocarcinoma (CHOL), stomach adenocarcinoma (STAD), and lung squamous cell carcinoma (LUSC) (Fig. 1A). A more detailed analysis revealed that, in comparison to normal tissues, MOSPD1 expression was significantly elevated in BC tissues ($P<0.001$; Fig. 1B). In another set of samples, MOSPD1 expression was also higher in BC tissues compared to corresponding normal tissues ($P<0.001$; Fig. 1C). The discriminative ability of MOSPD1 expression was further confirmed, with an AUC value of 0.766, indicating its potential application in distinguishing tumor tissues from normal tissues (Fig. 1D). Analysis of the TGCA database revealed a significant upregulation of MOSPD1 in BC. Studies focusing on prostate cancer also report elevated expression of MOSPD1 in tumor cells, regulated by the β-catenin/TCF7L2 complex [24]. Consequently, our decision to investigate the role of MOSPD1 in BC, along with the underlying mechanisms, was thus grounded in these findings.

Furthermore, using the STRING tool and Cytoscape software (v-3.8.0), we generated a PPI network for the MOSPD1 protein (Fig. 1E). A heatmap displayed the top 10 interacting proteins and their gene symbols (Fig. 1F). Proteins interacting with MOSPD1 included USP9X, STAG2, DDX3X, VAMP7, CUL4B, RAB1A, UBE2A, UBE2D1, THOC2, and UBQLN2, most of which are associated with cancer initiation, progression, and/or treatment. To further validate these findings, we performed immunohistochemical (IHC) staining using clinical samples. Interestingly, the IHC analysis revealed that MOSPD1 expression is primarily observed in infiltrating immune cells within the tumor microenvironment rather than in the tumor cells themselves. This observation further supports the potential role of MOSPD1 in modulating the tumor immune microenvironment, suggesting that it may influence tumor progression by promoting an immunosuppressive microenvironment. Representative IHC images are presented in Fig. 1G, further supporting the overexpression of MOSPD1 in tumors.

In summary, MOSPD1 consistently exhibited overexpression across various tumor types, especially in BC, highlighting its potential as a promising diagnostic biomarker for cancer detection and differentiation.

Impact of MOSPD1 expression on the growth of BC xenografts

To gain deeper insights into the role of MOSPD1 in BC progression, we undertook in vivo experiments to explore its potential regulatory effects on BC cell growth and apoptosis.

Subcutaneous injection of inhibitory or overexpressed MOSPD1 in BC MCF-7 and T47D cells was conducted. Throughout the experiment, we continuously monitored and documented the growth dynamics of these cell xenografts as well as the expression of MOSPD1. Immunohistochemistry results indicated that the protein levels of MOSPD1 decreased in the sh-MOSPD1 intervention group compared to the sh-NC control group in both MCF-7 and T47D cells ($P<0.01$). Conversely, in the oe-MOSPD1 intervention group, there was a significant increase in MOSPD1 protein expression compared to the oe-NC control group ($P<0.01$). Moreover, compared to the sh-MOSPD1+oe-NC group, the sh-MOSPD1+oe-MOSPD1 group showed increased MOSPD1 protein expression (Supplementary Fig. 1).

Further observations revealed that inhibiting MOSPD1 reduced the growth rate of MCF-7 and T47D xenografts, manifested as a pronounced reduction in tumor volume and weight ($P<0.01$) (Fig. 2A-C and Supplementary Fig. 2A-B). In contrast, overexpression of MOSPD1 promoted tumor growth. Additionally, compared to the sh-MOSPD1+oe-NC group, the sh-MOSPD1+oe-MOSPD1 group exhibited a significant increase in tumor size (Fig. 2A-C and Supplementary Fig. 2A-B). To further explore the mechanistic role of MOSPD1, we assessed the protein levels of Ki-67 in the tumor tissues, which serve as a cell proliferation marker. The data revealed that inhibition of MOSPD1 led to a significant decrease in the proportion of Ki-67 positive cells, while its overexpression significantly increased Ki-67 positive cells ($P<0.01$). The sh-MOSPD1+oe-MOSPD1 group exhibited a notably elevated tumor Ki-67 positivity rate compared to the sh-MOSPD1+oe-NC group (Fig. 2D and Supplementary Fig. 2C). Furthermore, we conducted TUNEL experiments to assess the impact of MOSPD1 on cell apoptosis. Our results revealed that inhibiting MOSPD1 increased the apoptosis rate of MCF-7 and T47D cell xenografts,

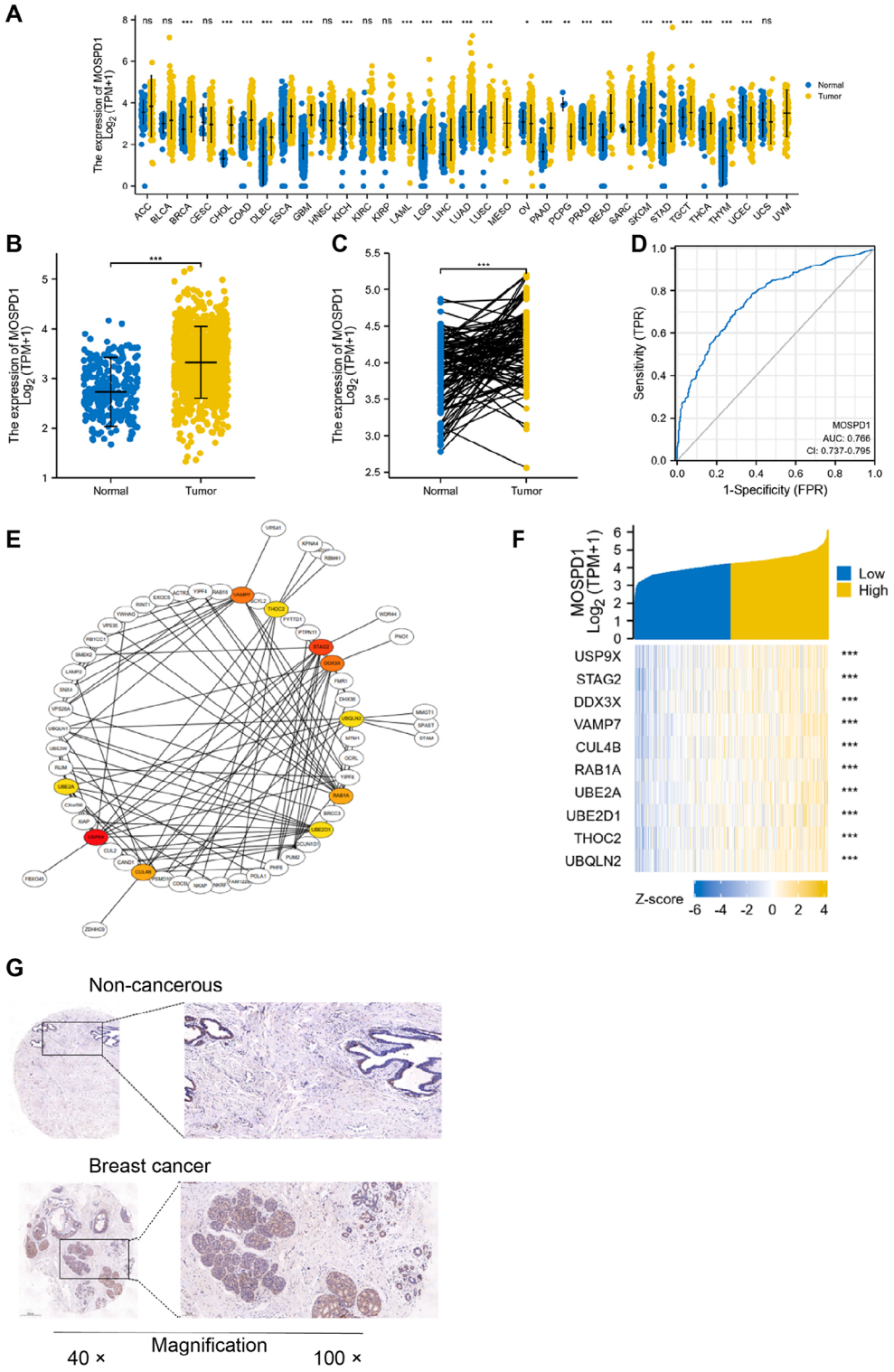

Fig. 1 Expression of MOSPD1 in different tumor types and breast cancer (BC) tissues and its diagnostic value for BC. *Note***(A)** Out of 33 tumor types, 19 show significantly higher expression of MOSPD1 than normal tissues. Legend: ***$p < 0.001$, **$p < 0.01$, *$p < 0.05$. **(B)** The difference in MOSPD1 expression levels between BC tissues and normal tissues. **(C)** Comparison of MOSPD1 expression between peritumoral tissues and BC tissues. **(D)** ROC curve analysis of MOSPD1, indicating significant diagnostic ability between BC and normal tissues. **(E)** Protein-protein interaction (PPI) network of MOSPD1. **(F)** A heatmap depicting the top 10 genes that exhibit significant co-expression between groups of high and low expression of MOSPD1. Blue to yellow represents downregulated and upregulated genes, respectively. **(G)** Representative immunohistochemistry (IHC) images of MOSPD1 in normal breast samples and BC tissues ($n = 44$)

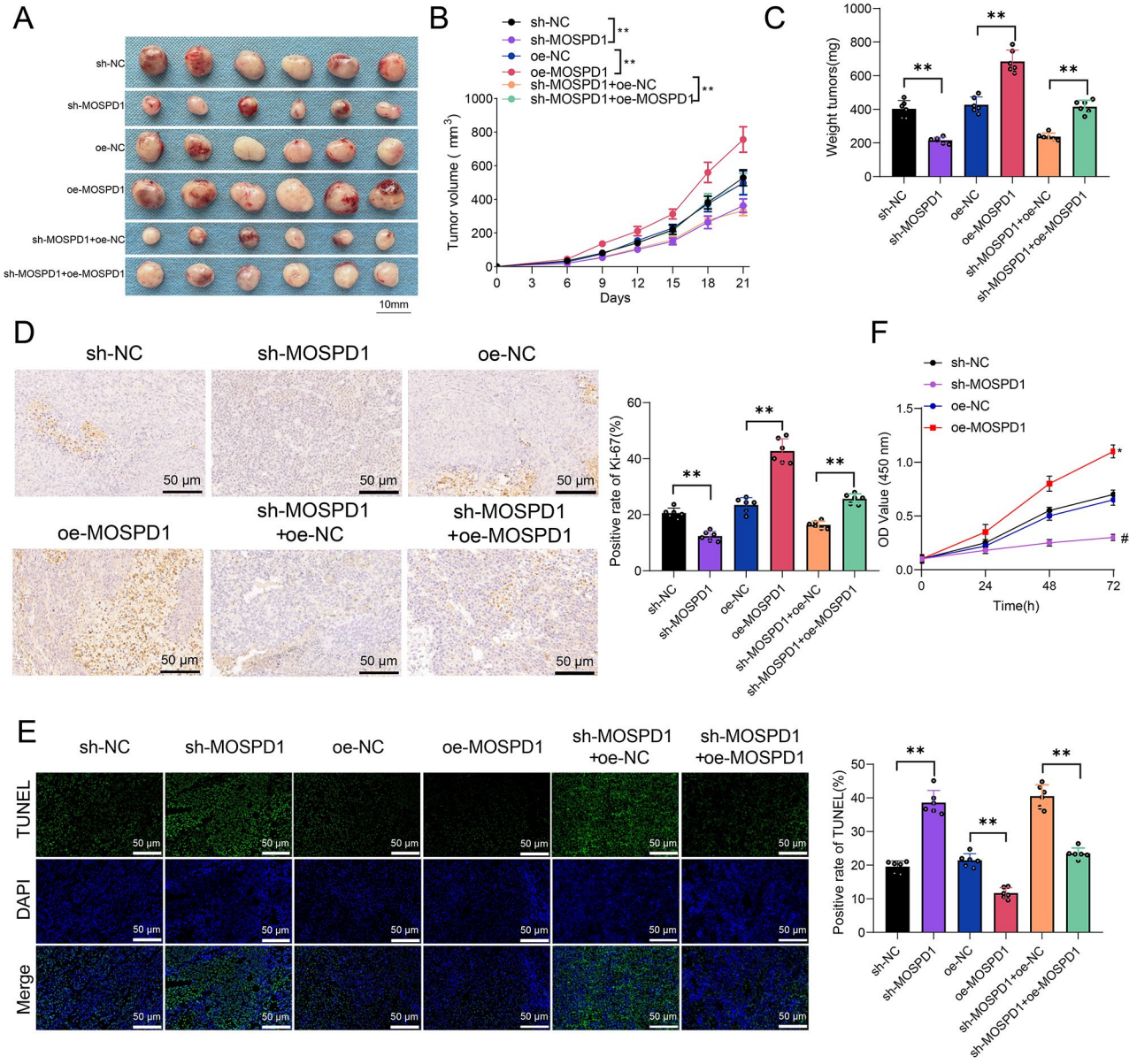

Fig. 2 Impact of MOSPD1 on the growth of MCF-7 cell-derived xenografts in BC. *Note***(A)** Photographs of xenografts formed by MCF-7 cells ($n=6$). **(B)** Influence of inhibiting or overexpressing MOSPD1 on the volume of MCF-7 cell-derived xenografts ($n=6$). **(C)** Influence of inhibiting or overexpressing MOSPD1 on the weight of MCF-7 cell-derived xenografts and quantitative analysis ($n=6$). **(D)** Immunohistochemistry detection and quantitative analysis of changes in Ki-67 positivity ($n=6$). **(E)** Immunofluorescence detection and analysis of TUNEL positivity changes ($n=6$). ** indicates $P<0.01$. **(F)** The effect of MOSPD1 knockdown or overexpression on MCF-7 cell viability detected by CCK-8 assay ($n=3$). */# indicates $P<0.01$ compared to the NC group

while overexpression of MOSPD1 reduced cell apoptosis ($P<0.01$). Compared to the sh-MOSPD1+oe-NC group, the sh-MOSPD1+oe-MOSPD1 group exhibited a marked decrease in tumor apoptosis rate (Fig. 2E and Supplementary Fig. 2D). Additionally, we are also interested in the role of MOSPD1 in vitro. Using the CCK-8 assay to assess cell viability, we found that knockdown of MOSPD1 resulted in decreased survival of MCF-7 and T47D cells, while overexpression led to increased cell viability (Fig. 2F and Supplementary Fig. 2E).

In conclusion, MOSPD1 significantly regulated the growth and apoptosis of BC MCF-7 and T47D cells in vivo, providing strong evidence for its pivotal role in BC progression and treatment.

Association analysis of MOSPD1 expression with clinical-pathological variables in BC

The study explored the associations between MOSPD1's expression and various clinical-pathological variables to further understand its role in BC.

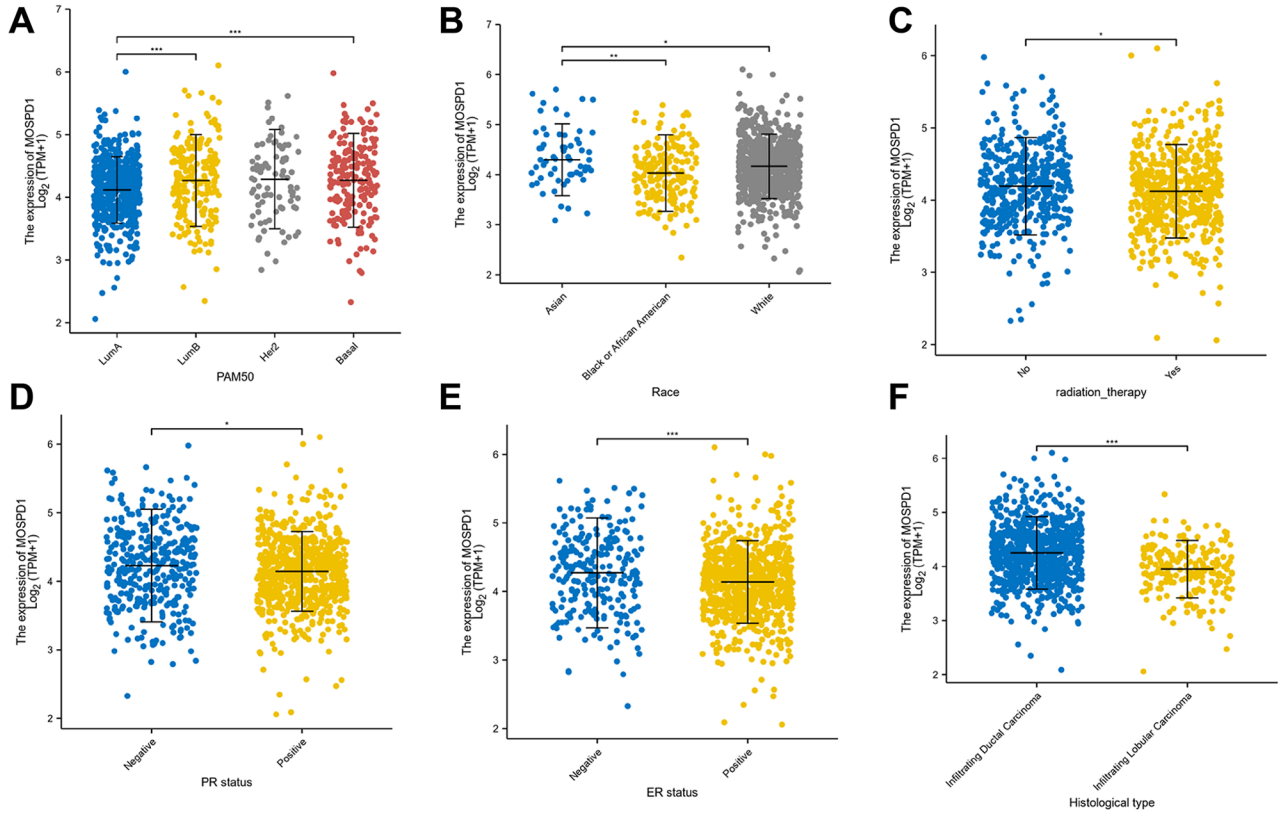

Fig. 3 Correlation between MOSPD1 expression and clinical pathological variables in BC. *Note***(A)** Association of MOSPD1 expression with PAM50 classification. **(B)** MOSPD1 expression concerning different ethnicities. **(C)** MOSPD1 expression about radiation therapy status. **(D)** MOSPD1 expression to PR status. **(E)** MOSPD1 expression concerning ER status. **(F)** MOSPD1 expression with different histological types

Table 3 Logistic analysis of the association between *MOSPD1* expression and clinical characteristics in BC patients

Characteristics	Total(*N*)	Odds Ratio(OR)	*P* value
T stage (T2&T3&T4 vs. T1)	1,080	1.227 (0.933–1.614)	0.144
N stage (N1&N2&N3 vs. N0)	1,064	1.405 (1.104–1.789)	0.006
M stage (M1 vs. M0)	922	1.761 (0.714–4.724)	0.232
Pathologic stage (Stage III&Stage IV vs. Stage I&Stage II)	1,060	1.124 (0.850–1.488)	0.413
Race (White vs. Asian&Black or African American)	994	1.174 (0.878–1.572)	0.279
Age (> 60 vs. <=60)	1,083	0.939 (0.739–1.193)	0.606
Histological type (Infiltrating Lobular Carcinoma vs. Infiltrating Ductal Carcinoma)	977	0.353 (0.253–0.489)	< 0.001
PR status (Positive vs. Negative)	1,030	0.778 (0.599–1.008)	0.058
ER status (Positive vs. Negative)	1,033	0.658 (0.491–0.881)	0.005
HER2 status (Positive vs. Negative)	715	1.167 (0.819–1.667)	0.393
Menopause status (Post vs. Pre)	932	1.054 (0.782–1.421)	0.730
Anatomic neoplasm subdivisions (Right vs. Left)	1,083	0.859 (0.677–1.091)	0.213
radiation_therapy (Yes vs. No)	987	0.782 (0.608–1.006)	0.055

The Kruskal-Wallis rank-sum analysis showed that MOSPD1 expression levels were significantly associated with PAM50 classification and patient ethnicity (all $P<0.05$). The Wilcoxon rank-sum test further confirmed significant associations between MOSPD1 expression and radiation therapy, PR status, ER status, and histological type (all $P<0.05$) (Fig. 3).

We employed logistic regression analysis to gain deeper insights into the relationship between MOSPD1 expression and adverse clinical features predicting poor prognosis. The results indicated significant associations of MOSPD1 expression with N stage (N1&N2&N3 vs. N0) (OR=1.405, 95% Confidence Interval [CI]=1.104–1.789, $p=0.006$), histological type (invasive lobular carcinoma vs. invasive ductal carcinoma) (OR=0.353, 95%CI=0.253–0.489, $p<0.001$), and ER status (positive vs. negative) (OR=0.658, 95%CI=0.491–0.881, $p=0.005$) (Table 3).

Overall, MOSPD1 expression demonstrated significant relationships with multiple clinical-pathological variables in BC, further emphasizing its potential importance in the pathogenesis of BC (See Table 3).

Prognostic implications of MOSPD1 expression levels

The significance of MOSPD1 expression in BC has been preliminarily explored. We conducted a series of survival analyses and statistical assessments to discern its role in BC prognosis further.

Kaplan-Meier survival curve analysis unveiled the role of MOSPD1 in BC prognosis. Specifically, patients with high MOSPD1 expression levels displayed significantly poorer overall survival than those with low MOSPD1 expression levels (Fig. 4A). This adverse prognostic trend was also confirmed in the progression-free interval (PFI), as high MOSPD1 expression was significantly associated with shorter PFI (Fig. 4B). Subgroup analysis based on HER2 status revealed that MOSPD1 expression level was a significant prognostic indicator. For HER2-negative BC patients, high MOSPD1 expression was linked to shorter overall survival (hazard ratio [HR] = 2.00, $P = 0.008$, Fig. 4C). Similarly, in HER2-positive BC patients, high MOSPD1 expression also indicated an unfavorable prognosis (HR = 3.28, $P = 0.01$, Fig. 4D). These findings suggest that MOSPD1 expression levels are an independent prognostic marker regardless of HER2 status.

We further employed univariate and multivariate Cox regression models for analysis. The univariate analysis indicated that MOSPD1 (Hazard Ratio [HR] = 1.557, $p = 0.008$), T stage (HR = 1.608, $p = 0.012$), age (HR = 2.022, $p < 0.001$), M stage (HR = 4.254, $p < 0.001$), and N stage (HR = 2.163, $p < 0.001$) were prognostic factors for BC (Fig. 4E). In the multivariate model, MOSPD1 (HR = 1.681, *$p = 0.046$)*, T stage (HR = 2.307, $p = 0.01$), and age (HR = 3.198, $p < 0.001$) were identified as independent prognostic factors for BC (Fig. 4F).

Combining these three independent prognostic factors, MOSPD1, T stage, and age, we established a risk-scoring model to predict 1-year, 3-year, and 5-year OS for BC patients (Fig. 4G). As the risk scores increased, the patients' prognoses worsened. The calibration curve of this model confirmed its accuracy in predicting 1-year, 3-year, and 5-year OS (Fig. 4H).

Taken together, not only is the expression level of MOSPD1 significantly correlated with poor prognosis in BC, but it has also been validated as an independent prognostic factor, providing pivotal evidence for its clinical utility.

Association between MOSPD1 expression and BC gene expression profiles and its role in immune pathways

To delve deeper into the functional role of MOSPD1 in BC and its potential regulatory mechanisms, we utilized TCGA datasets for differential gene expression analysis and further explored its relationship with immune-related pathways.

The study conducted a comparative analysis of high and low MOSPD1 expression in BC samples using the R package DESeq2, identifying significant differentially expressed genes (DEGs). With a threshold of |log2 fold change (logFC)| > 1 and an adjusted P-value of 0.05, 2965 DEGs were identified. Among samples with high MOSPD1 expression, 221 genes like UGT2B4 and GLYATL3 were significantly upregulated, while 2744 genes, including SNORA73B and RNU1-139P, were notably downregulated (Fig. 5A). A heatmap depicted the expression patterns of these DEGs, emphasizing changes in crucial genes like FGF4 involved in immune regulation and cell signaling pathways (Fig. 5B).

The study aimed to investigate the potential functional role of MOSPD1 in BC by comparing gene expression differences between high and low MOSPD1 expression samples. Gene set enrichment analysis (GSEA) revealed significant enrichment of immune-related gene sets in samples with low MOSPD1 expression, such as immune modulation post-HCMV infection, primary immunodeficiency, and complement cascade pathways (Fig. 5C). This finding suggests possible immune activation in the tumor microenvironment with low MOSPD1 expression. Conversely, in samples with high MOSPD1 expression, there was a substantial downregulation of immune regulation pathways, indicating a potential weakening of immune surveillance by MOSPD1 through the suppression of vital immune genes (Fig. 5C). This suppression may lead to cytokine and chemical factor expression alterations, impacting immune cell infiltration and activity.

In conclusion, MOSPD1 expression in BC is associated with differential expression of many genes, particularly with significant enrichment in immune-related pathways, offering insights into the potential role of MOSPD1 in the immune modulation of BC.

Impact of MOSPD1 on immune cell infiltration and Th2 cell activity in BC

Given this, to determine the influence of MOSPD1 expression on immune cell infiltration and the tumor microenvironment, we employed ssGSEA for immune infiltration analysis. Using Spearman correlation analysis, we computed the relationship between immune cell enrichment in BC tissues and MOSPD1 expression levels (Fig. 6A). The results showed that Th2 cells, Central Memory T cells (TCM), Gamma Delta T cells (Tgd), T-helper cells, and macrophages were positively correlated with MOSPD1 expression levels (Fig. 6B-F), with the correlation coefficient being the largest for Th2 cells.

Th2 cells in BC tumor tissues were assessed using flow cytometry. Results indicated a significant reduction in

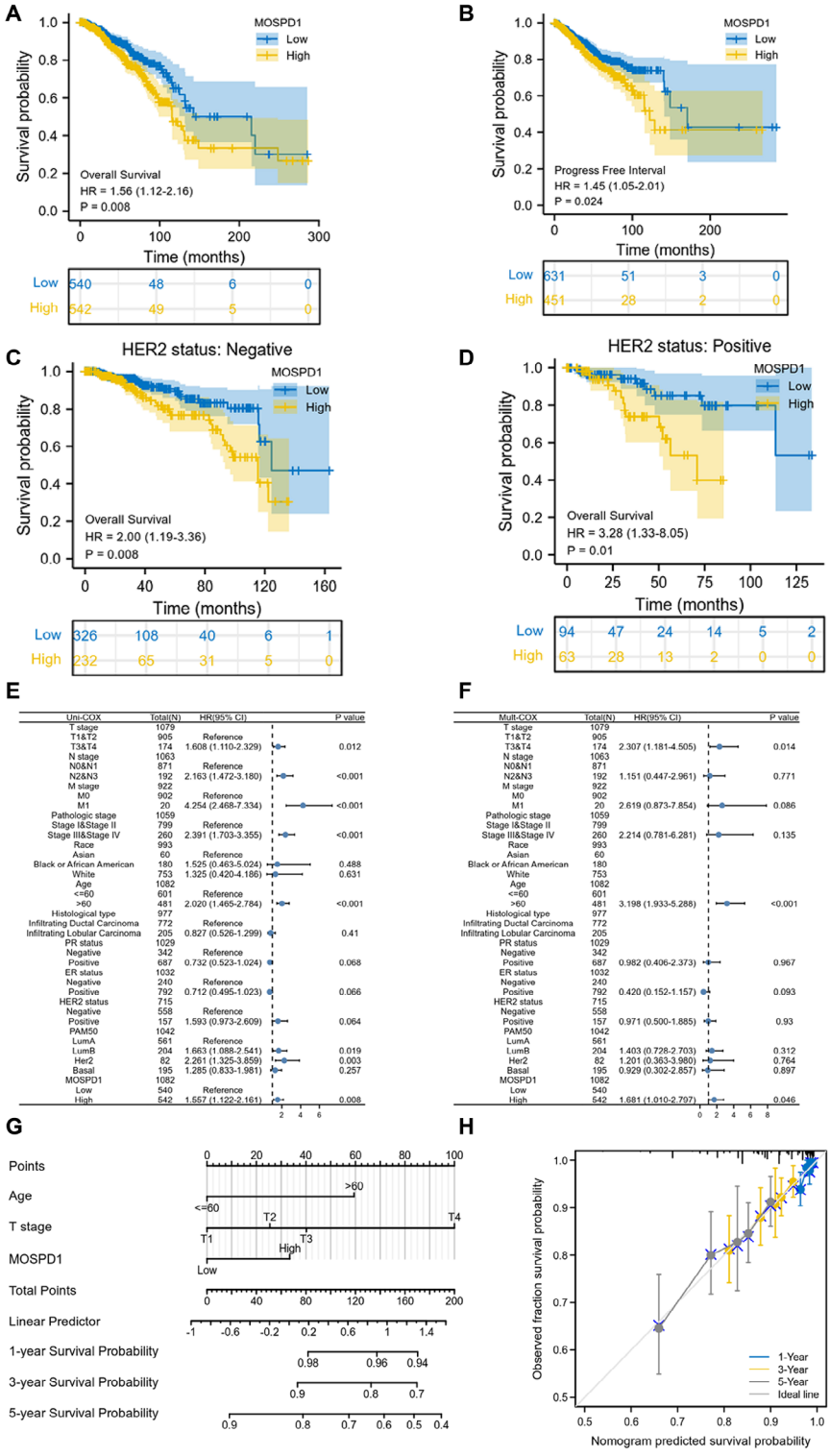

Fig. 4 Analysis of the correlation between MOSPD1 expression levels and prognosis in BC. *Note***(A-B)** Kaplan-Meier survival curves for BC patients with high and low MOSPD1 expression: **(A)** Overall survival rate; **(B)** Progression-free survival period. (C-D) Subgroup analysis based on HER2 status: **(C)** Overall survival rate in HER2-negative patients; **(D)** Overall survival rate in HER2-positive patients. **(E-F)** Association of MOSPD1 expression levels with prognosis in BC: **(E)** Univariate Cox regression analysis results; **(F)** Multivariate Cox regression analysis results. **(G-H)** Prediction of prognosis in BC patients combining MOSPD1 expression with other clinical variables: **(G)** Predicted 1-year, 3-year, and 5-year overall survival rates using the risk scoring model; **(H)** Calibration curve of the model verifying prediction accuracy

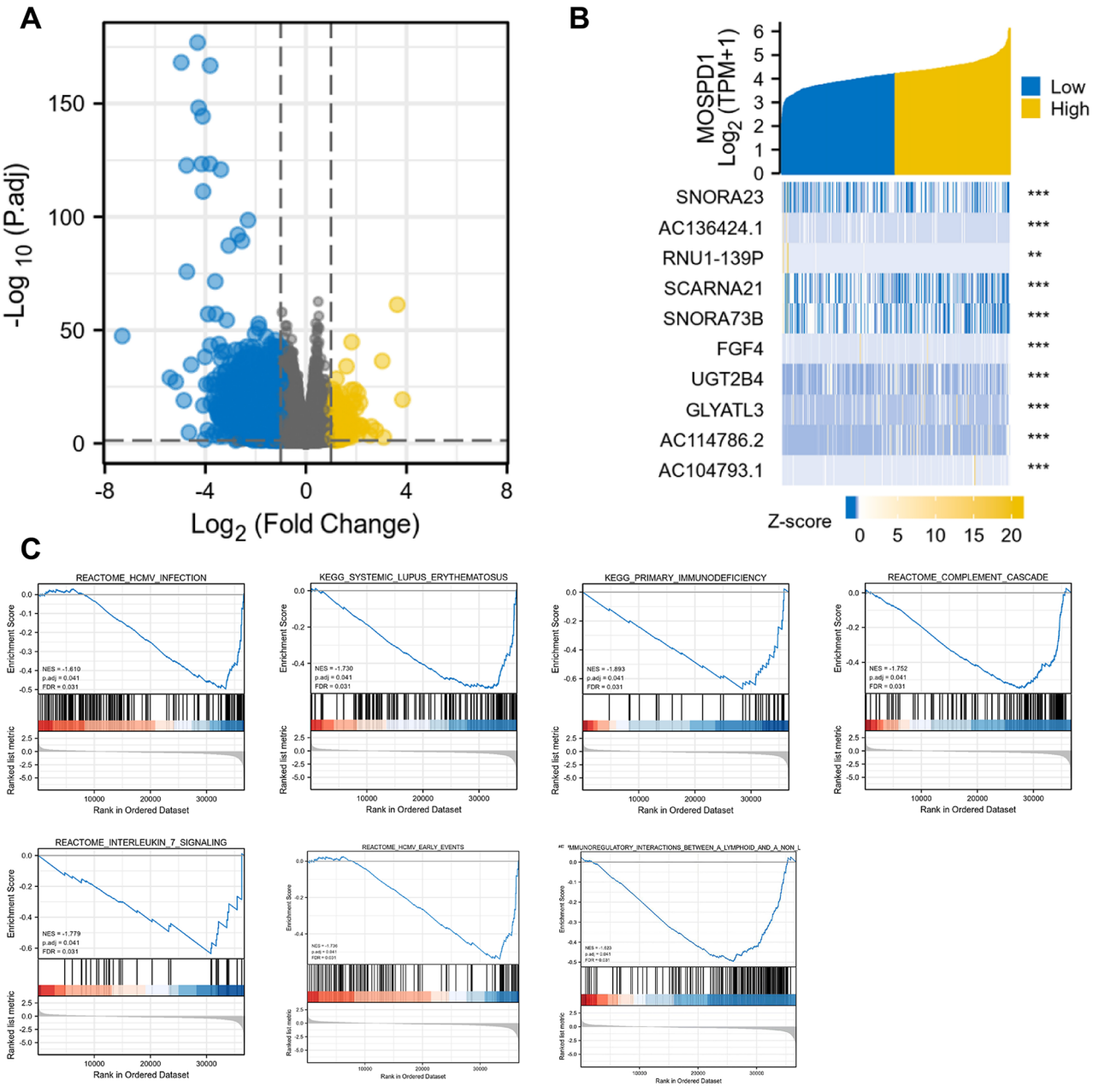

Fig. 5 Correlation between MOSPD1 expression in BC and differentially expressed genes and biological pathways. *Note* **(A)** Volcano plot showcasing differentially expressed genes between BC patients with high and low MOSPD1 expression. Gene standardized expression levels are represented from blue (low) to yellow (high). **(B)** Bar chart displaying the top 10 significantly differentially expressed genes based on MOSPD1 expression levels. Blue represents downregulated genes, and yellow represents upregulated genes. **(C)** GSEA analysis results show significantly enriched biological pathways in the MOSPD1 low-expression group. NES stands for normalized enrichment score

the number of Th2 cells in MOSPD1-silenced MCF-7 and T47D tumors compared to the control group, while there was an increase in the abundance of these cells in MOSPD1-overexpressed MCF-7 and T47D tumors ($P<0.01$) (Fig. 6G-H and Supplementary Fig. 3A-B). Furthermore, the relative mRNA expression levels of IL-4, IL-5, and IL-13 in tumor tissues of MOSPD1-silenced MCF-7 and T47D groups were decreased, whereas the mRNA levels of these cytokines were elevated in MOSPD1-overexpressed MCF-7 and T47D tumors ($P<0.01$) (Fig. 6I and Supplementary Fig. 3C).

In summary, MOSPD1 expression in BC is closely related to immune cell infiltration, especially the activity of Th2 cells. Specifically, the silencing of MOSPD1 suppressed Th2 cell activity, while its overexpression enhanced Th2 cell functions.

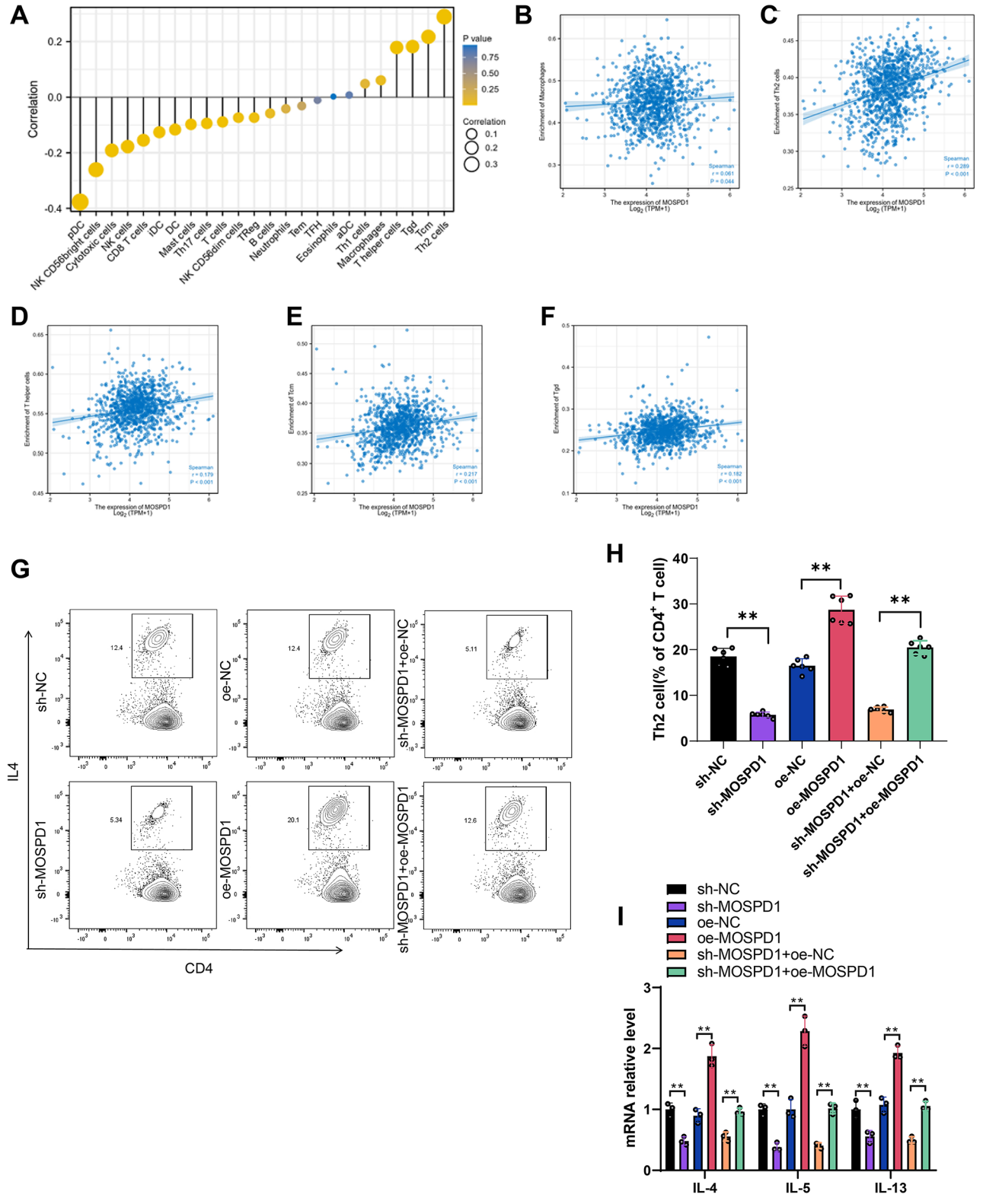

Fig. 6 Analysis of the correlation between MOSPD1 expression and the level of immune cell infiltration in BC. *Note* **(A)** Analysis of the correlation between MOSPD1 expression and the infiltration level of 24 types of immune cells. **(B-F)** Detailed correlation graphs between MOSPD1 expression and infiltration levels of Th2 cells, Tcm, Tgd, T helper cells, and macrophages. **(G-H)** Flow cytometry detection and quantitative analysis of the effect of silencing or overexpressing MOSPD1 on Th2 cell numbers in tumor tissues of BC cell-derived xenografts ($n=6$). **(I)** Impact of silencing MOSPD1 on the relative mRNA expression levels of IL-4, IL-5, and IL-13 in Th2 cells of BC cell-derived xenograft tumor tissues ($n=6$). ** indicates $P<0.01$

Analysis of MOSPD1 expression about BC microenvironment and immune checkpoints

Following our earlier studies on the correlation between MOSPD1 and immune cell infiltration in BC, we further explored the relationship between MOSPD1, the tumor microenvironment, and immune checkpoints.

Initially, we utilized the ESTIMATE algorithm to analyze the stromal score, immune score and estimate score in BC. We found that MOSPD1 expression had a significant negative correlation with all three (*P<0.001*) (Fig. 7A). Additionally, we delved deeper into the association between MOSPD1 and various immune checkpoints. Data revealed that MOSPD1 expression had significant relationships with multiple critical immune checkpoint genes, such as TNFRSF14, PD-L1, TNFSF4, B7-H2, and TNFRSF4, implying a pivotal role for MOSPD1 in immune therapy responses (Fig. 7B). Notably, PD-L1 (CD274), an immune checkpoint protein, has been associated with poor prognosis in various cancers, especially BC [25–27].

Based on the results and the analysis above, we hypothesize that MOSPD1 may synergize with the PD-L1 protein, modulating Th2 cell activity and promoting the tumorigenesis of BC cells in mice.

Silencing MOSPD1 enhances sensitivity of BC MCF-7 Cells to Anti-PD-L1 and synergistically suppresses Th2 cell activity

After reviewing the literature, we discovered that studies have found high expression of PD-L1 protein in MCF-7 cells [28] and that Th2 cells may impact the tumor microenvironment and immune cell function [29, 30]. Furthermore, research indicates that PD-L1 expression is influenced by MOSPD1 [30]. Therefore, we investigated whether MOSPD1 affects the activity of Th2 cells or influences PD-L1 sensitivity, consequently affecting the development of BC. Based on these hypotheses, we evaluated the impact of MOSPD1 on the sensitivity of MCF-7 and T47D BC cell xenografts to anti-PD-L1 treatment.

The experiment was divided into eight groups: sh-NC, sh-NC+anti-PD-L1, sh-MOSPD1, sh-MOSPD1+anti-PD-L1, oe-NC, oe-MOSPD1, oe-NC+anti-PD-L1, and oe-MOSPD1+anti-PD-L1, to assess the effects of MOSPD1 expression on MCF-7 and T47D BC cell xenografts and their sensitivity to anti-PD-L1. Compared to the sh-NC+anti-PD-L1 or sh-MOSPD1 groups, the sh-MOSPD1+anti-PD-L1 group exhibited further suppression of tumor growth, volume, and weight *(P<0.01)*. In contrast, compared to the oe-NC group, the oe-MOSPD1 group showed a significant increase in tumor growth, volume, and weight *(P<0.01)*, with no significant difference observed between the oe-MOSPD1+anti-PD-L1 group and the oe-MOSPD1 group (Fig. 8A-C and Supplementary Fig. 4A-C).

Ki-67 is a marker of cell proliferation. Thus, we examined the expression of Ki-67 in tumor tissues of different treatment groups. Results indicated that compared to the sh-NC group, the sh-NC+anti-PD-L1 and sh-MOSPD1 groups showed a reduction in Ki-67 positivity, indicating suppression of cell proliferation (*P<0.01*). In

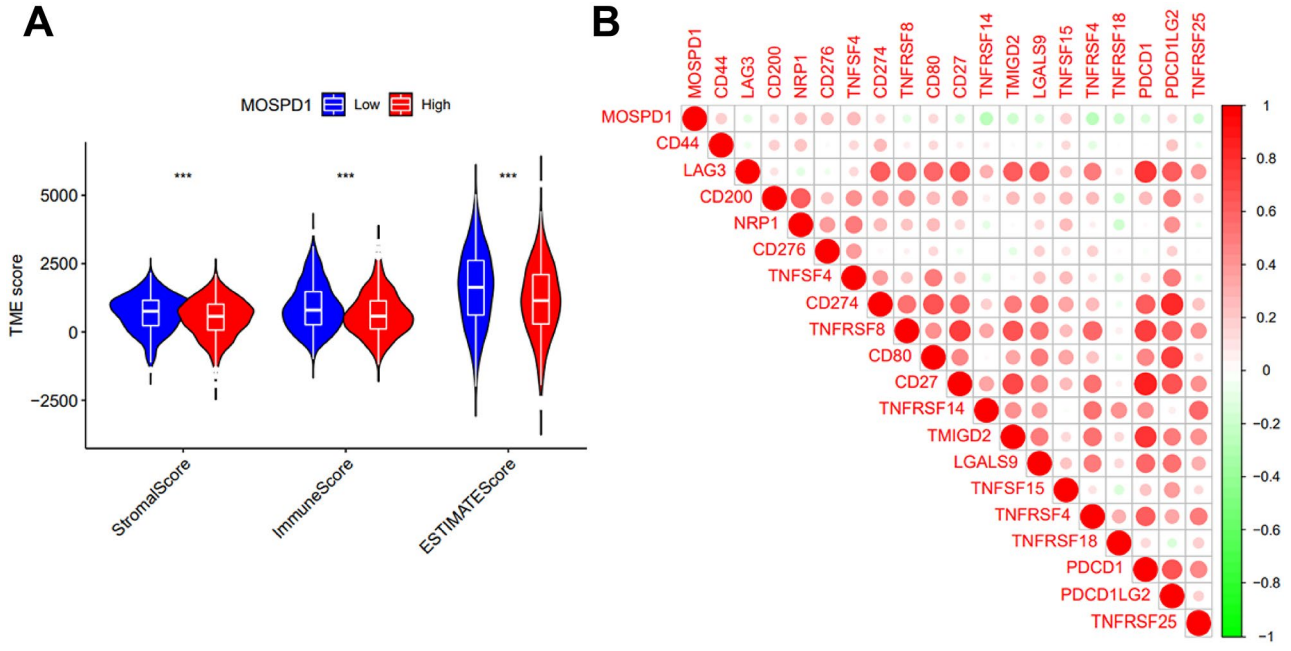

Fig. 7 Display the association of MOSPD1 expression with the BC microenvironment and immune checkpoints. *Note* **(A)** Relationship between MOSPD1 expression levels and stromal score, immune score, and estimate score in BC. **(B)** Correlation analysis between MOSPD1 and the expression of key immune checkpoint genes, with CD274 representing PD-L1

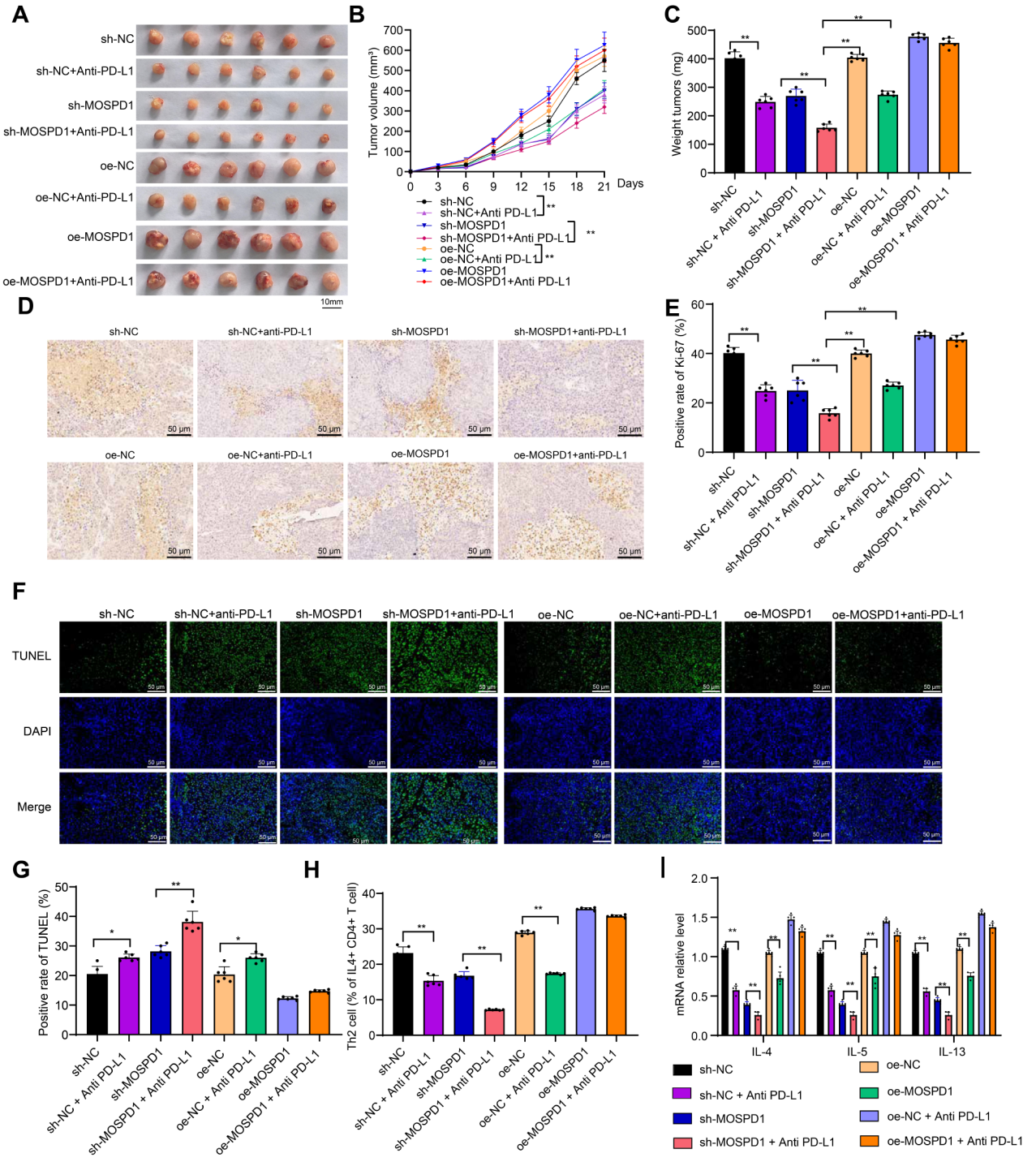

Fig. 8 Impact of MOSPD1 on the drug sensitivity of Anti-PD-L1 in MCF-7 cell-derived xenografts in BC. *Note* **(A)** Comparative photographs of xenografts from sh-NC, sh-MOSPD1, and sh-MOSPD1 + Anti-PD-L1 groups of BC MCF-7 cells ($n = 6$). **(B)** Comparative analysis of the effect on the volume of MCF-7 cell-derived xenografts in sh-NC, sh-MOSPD1, and sh-MOSPD1 + Anti-PD-L1 groups ($n = 6$). **(C)** Comparative analysis of the effect on the weight of MCF-7 cell-derived xenografts in sh-NC, sh-MOSPD1, and sh-MOSPD1 + Anti-PD-L1 groups ($n = 6$). **(D-E)** Immunohistochemistry validation and quantitative analysis of changes in Ki-67 in MCF-7 cell-derived xenografts with MOSPD1 inhibition and Anti-PD-L1 intervention ($n = 6$). **(F-G)** Immunofluorescence validation and quantitative analysis of inhibiting MOSPD1 and Anti-PD-L1 effects on TUNEL in MCF-7 cell-derived xenografts ($n = 6$). **(H)** Flow cytometry detection and quantitative analysis of the effect of MOSPD1 silencing on Th2 cell numbers in tumor tissues of BC cell-derived xenografts ($n = 6$). **(I)** Impact of silencing MOSPD1 on the relative mRNA expression levels of IL-4, IL-5, and IL-13 in Th2 cells of BC cell-derived xenograft tumor tissues ($n = 6$). ** indicates $P < 0.01$

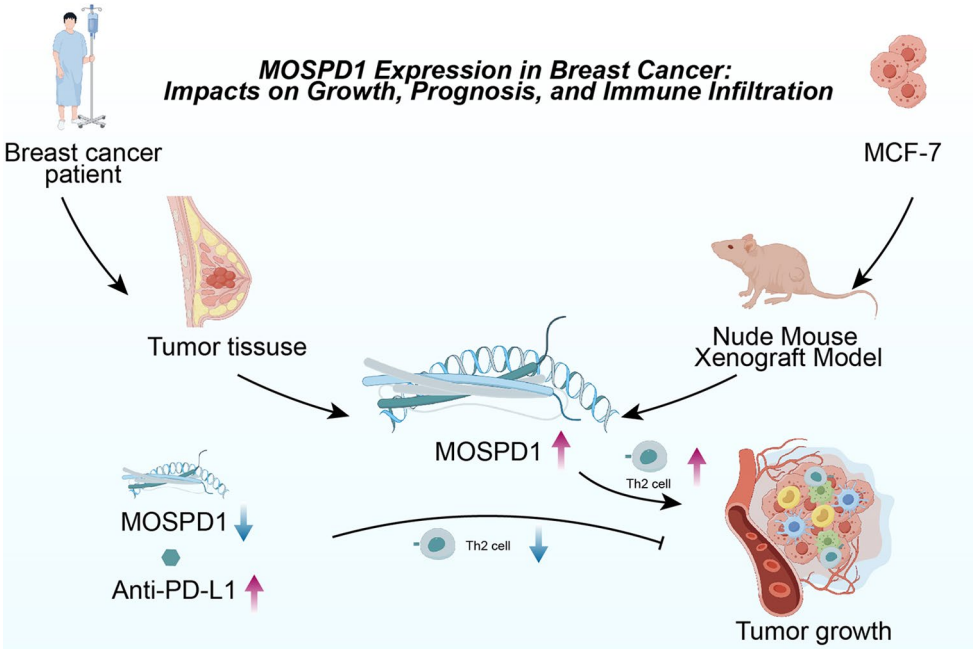

Fig. 9 Overview of the expression of MOSPD1 and its relationship with immune infiltration in BC

contrast, the sh-MOSPD1+anti-PD-L1 group exhibited a further decrease in Ki-67 positivity compared to the sh-NC+anti-PD-L1 or sh-MOSPD1 groups ($P<0.01$). In comparison to the oe-NC group, the Ki-67 positivity rate was increased in the oe-MOSPD1 group ($P<0.01$), with no significant difference observed between the oe-MOSPD1+anti-PD-L1 group and the oe-MOSPD1 group. (Fig. 8D-E, Supplementary Fig. 4D-E).

TUNEL staining results revealed a significant increase in TUNEL positivity in tumor tissues of the sh-NC+anti-PD-L1 and sh-MOSPD1 groups compared to the sh-NC group, indicating increased cell apoptosis ($P<0.01$). Furthermore, compared to the sh-NC+anti-PD-L1 or sh-MOSPD1 groups, the sh-MOSPD1+anti-PD-L1 group displayed a further increase in TUNEL positivity in tumor tissues ($P<0.01$). In contrast to the oe-NC group, the Ki-67 positivity rate was decreased in the oe-MOSPD1 group ($P<0.01$), with no significant difference observed between the oe-MOSPD1+anti-PD-L1 group and the oe-MOSPD1 group. (Fig. 8F-G, Supplementary Fig. 4F-G).

Furthermore, flow cytometry was used to detect Th2 cells in BC tumor tissues. Experimental results revealed a significant decrease in the proportion of Th2 cells in the sh-NC+anti-PD-L1 and sh-MOSPD1 groups compared to the sh-NC group. Moreover, compared to the sh-NC+anti-PD-L1 or sh-MOSPD1 groups, the proportion of Th2 cells in tumor tissues was further reduced in the sh-MOSPD1+anti-PD-L1 group ($P<0.01$). Compared to the oe-NC group, the proportion of Th2 cells was significantly higher in the oe-MOSPD1 group. The proportion of Th2 cells in the tumor tissues of the oe-NC+anti-PD-L1 and sh-MOSPD1+anti-PD-L1 groups was further significantly increased, with no significant difference observed when compared to the oe-MOSPD1 group ($P<0.01$) (Fig. 8H, Supplementary Fig. 4H). Evaluation of the expression of IL-4, IL-5, and IL-13 in tumor tissues revealed that mRNA levels of these cytokines were decreased in the sh-NC+anti-PD-L1 and sh-MOSPD1 groups compared to the sh-NC group ($P<0.01$). Additionally, the sh-MOSPD1+anti-PD-L1 group exhibited a further reduction in mRNA levels of IL-4, IL-5, and IL-13 in tumor tissues compared to the sh-NC+anti-PD-L1 or sh-MOSPD1 groups. Compared to the oe-NC group, the oe-MOSPD1 group showed an increase in the relative mRNA expression levels of IL-4, IL-5, and IL-13. The relative mRNA expression levels in the tumor tissues of the oe-NC+anti-PD-L1 and sh-MOSPD1+anti-PD-L1 groups were elevated as well, with no significant difference compared to the oe-MOSPD1 group *($P<0.01$)* (Fig. 8I, Supplementary Fig. 4I).

The above results indicate that inhibiting MOSPD1 can enhance the sensitivity of breast cancer MCF-7 and T47D cells to anti-PD-L1 treatment, while overexpression of MOSPD1 reduces the sensitivity of these cells to anti-PD-L1. This effect may be mediated through the synergistic inhibition of Th2 cell activity.

Discussion

Breast cancer (BC) is the most prevalent malignant tumor among women worldwide, accounting for 24.5% of female tumor incidences, surpassing lung cancer [31].

Currently, chemotherapy, often combined with surgery or radiotherapy, is the principal treatment method for BC [32]. However, many patients experience recurrence or malignant progression due to BC's highly invasive nature. It searches for effective prognostic biomarkers and immunotherapeutic targets paramount [33].

In recent years, the expression and role of MOSPD1 in various cancers have gained widespread attention [17, 34]. In some cancers, MOSPD1 expression is significantly elevated, while in others, it is relatively lower, possibly due to differences in the biological characteristics of these cancers or the mechanisms by which MOSPD1 functions in them. Our study found that MOSPD1 expression is significantly higher in breast cancer tissues than in normal tissues, with higher levels in MCF-7 cells than in T47D cells (supplementary materials). This finding suggests a key role for MOSPD1 in breast cancer, potentially related to the enhanced proliferation and invasiveness of MCF-7 cells. The differential expression of MOSPD1 underscores its potential therapeutic value in breast cancer, warranting further investigation.

The growth and metastasis of BC profoundly impact patient prognosis [35, 36]. Our research focused on the potential association between MOSPD1 and BC growth and metastasis. Experimental outcomes demonstrated that inhibiting MOSPD1 slowed the growth of BC MCF-7 and T47D cell xenografts, whereas its overexpression expedited this process. It provides evidence of MOSPD1's pivotal role in BC growth and metastasis. Simultaneously, based on TCGA and GTEx data, we assessed MOSPD1 expression levels in pancreatic cancer and BC. In 19 cancer types, including breast cancer (BC), MOSPD1 expression was significantly elevated, and it was found to be basally expressed at relatively high levels in both MCF7 and T47D cell lines. ROC curve results indicate that MOSPD1 holds a decent diagnostic value (AUC=0.766). Moreover, using clinical samples, IHC results confirmed the elevated expression of MOSPD1 in BC compared to adjacent tissues. Subsequently, we evaluated how MOSPD1 might influence the prognosis of BC patients. According to OS and PFI analysis, MOSPD1 significantly correlates with BC patient outcomes and acts as a risk factor for BC. Both univariate and multivariate Cox regression analyses pinpointed MOSPD1 as an independent prognostic marker, playing a critical role in predicting its prognosis.

Immune cell infiltration within the tumor microenvironment plays a pivotal role in cancer progression [37]. In BC, immune cell infiltration is intimately linked with disease prognosis and treatment response [11, 38]. In this study, based on GSEA outcomes, there's a close association between MOSPD1 and immune activation processes, such as immune regulatory interactions between lymphoid and non-lymphoid cells, HCMV infection, systemic lupus erythematosus, early events in HCMV, and primary immunodeficiency. Certain studies have found that immune-related pathways, such as HCMV infection, primary immunodeficiency, and immune regulatory interactions between lymphoid and non-lymphoid cells, play an irreplaceable role in predicting cancer prognosis, immune infiltration, and the immune therapeutic response in cancer [39–41].

One of our crucial findings is that MOSPD1 expression is also highly correlated with immune infiltration in BC. MOSPD1 is positively associated with the infiltration level of Th2 cells, Tcm, Tgd, T-helper cells, and macrophages in BC. Animal studies indicate a close relationship between MOSPD1 expression and immune cell infiltration, especially the activity of Th2 cells. The high expression of MOSPD1 in Th2 cells may play a crucial role in promoting an immunosuppressive microenvironment and tumor immune evasion. Th2 cells inhibit antitumor immune responses by secreting cytokines such as IL-4, IL-5, and IL-13 [42]. MOSPD1 may support tumor growth and progression by enhancing Th2 cell activity.

Additionally, we observed that MOSPD1 expression is associated with resistance to anti-PD-L1 therapy in xenograft models. MOSPD1 may weaken the efficacy of immune checkpoint inhibitors by regulating Th2 cells and other immunosuppressive mechanisms. Therefore, targeting MOSPD1 or its downstream signaling pathways could enhance the effectiveness of anti-PD-L1 therapy, particularly in breast cancer patients who respond poorly to existing immunotherapies. These findings provide new insights into the immune response in breast cancer and suggest new directions for immunotherapy.

PD-L1 has recently emerged as a significant target for BC immunotherapy [43]. The efficacy of anti-PD-L1 is closely related to the activity of specific molecules and pathways within the tumor [44–46]. Our study identified a relationship between MOSPD1 expression and the drug sensitivity to anti-PD-L1. It provides robust evidence for MOSPD1 as a novel target for BC immunotherapy.

Indeed, this study has its limitations. We primarily relied on the TCGA database, which may introduce data biases, and the experiments were only conducted on MCF-7 and T47D cell lines. These limitations could potentially impact the results and conclusions of our study. While our findings suggest that MOSPD1 plays a crucial role in regulating cell proliferation and apoptosis in BC cells, the direct determination of MOSPD1's role in BC cells through post-sequencing analysis was hindered by financial constraints, presenting a limitation of this study. However, we believe these initial discoveries lay a crucial groundwork for future research. Looking ahead, we aim to incorporate a broader range of BC patient samples and other BC cell lines in our investigations. By conducting more comprehensive experiments and

clinical studies, we can better understand the proper role of MOSPD1 in BC. Additionally, we intend to delve into the molecular mechanisms of MOSPD1 and explore the development of treatment strategies based on MOSPD1.

In summary, our research offers profound insights and novel findings. We explored MOSPD1's expression and function and revealed its relationship with Th2 immune cell infiltration and drug sensitivity to anti-PD-L1 (Fig. 9). These new findings grant us a fresh perspective, allowing a more comprehensive understanding of MOSPD1's role in BC. Of course, compared to other studies, our research also showcases differences. These variances might be attributed to experimental methodologies, sample sources, or other conditions. Future research can further juxtapose these differences and probe their potential reasons. By comparing results from diverse studies, we can better understand the genuine role of MOSPD1 in BC. Overall, compared to other research, our study provides a new perspective and inspiration for BC research.

Supplementary Information

The online version contains supplementary material available at https://doi.org/10.1186/s13062-024-00531-9.

Supplementary Material 1: Supplementary Fig. 1. Immunohistochemistry detection of MOSPD1 expression in BC. Note: Immunohistochemistry was performed to detect MOSPD1 expression levels in xenograft tumors of MCF-7 and T47D BC cells, showing the efficiency of silencing or overexpression. ** indicates $P < 0.01$.

Supplementary Material 2: Supplementary Figure 2. The Impact of MOSPD1 on BC T47D Xenograft Growth. Note: (A) Effects of inhibiting or overexpressing MOSPD1 on the volume of T47D cell xenograft tumors ($n = 6$). (B) Influence of inhibiting or overexpressing MOSPD1 on the mass of T47D xenograft tumors, including quantitative analysis ($n = 6$). (C) Immunohistochemical examination of Ki-67 variations, with analysis and quantification of Ki-67 positivity rate ($n = 6$). (D) Immunofluorescence detection of TUNEL variations and analysis of positivity rate. (E) The effect of MOSPD1 knockdown or overexpression on T47D cell viability detected by CCK-8 assay ($n = 3$). */# indicates $P < 0.01$ compared to the NC group.

Supplementary Material 3: Supplementary Figure 3. Analysis of the Impact of MOSPD1 on Th2 Infiltration in Tumor Tissues in BC T47D Cells. Note: (A-B) Flow cytometry was utilized to assess the influence of MOSPD1 knockdown or overexpression on the quantity of Th2 cells in the tumor tissues of BC T47D xenografts, presented in contour plots and quantified analysis ($n = 6$). (C) The impact of MOSPD1 knockdown or overexpression on the relative mRNA expression levels of IL-4, IL-5, and IL-13 in Th2 cells within the tumor tissues of BC T47D xenografts was examined ($n = 6$). ** represents $P < 0.01$.

Supplementary Material 4: Supplementary Figure 4. Impact of MOSPD1 on the Sensitivity of BC T47D Xenografts to Anti-PD-L1 Treatment. Note: (A) Comparison of physical images of T47D breast cancer cell xenografts among different groups ($n = 6$). (B) Comparison of the effects on T47D breast cancer cell xenograft volume among different groups ($n = 6$). (C) Comparison of the effects on the weight of T47D breast cancer cell xenografts among different groups ($n = 6$). (D-E) Immunohistochemical validation and quantitative analysis of the effects of MOSPD1 inhibition or overexpression on Ki-67 in T47D breast cancer cell xenografts with Anti-PD-L1 intervention ($n = 6$). (F-G) Immunofluorescence validation and quantitative analysis of the effects of MOSPD1 inhibition or overexpression on TUNEL assay in T47D breast cancer cell xenografts treated with Anti-PD-L1 ($n = 6$). (H) Contour plots and quantitative analysis of the effects of MOSPD1 silencing or overexpression on the number of Th2 cells in tumor tissues of T47D breast cancer cell xenografts detected by flow cytometry ($n = 6$). (I) The effect of MOSPD1 silencing or overexpression on the relative mRNA expression levels of IL-4, IL-5, and IL-13 in Th2 cells within the tumor tissues of T47D breast cancer cell xenografts ($n = 6$).

Supplementary Material 5

Acknowledgements
Not applicable.

Author contributions
Yiling Jiang and Hailong Li were responsible for conceptualizing the study, performing RNA-seq analysis, and interpreting data. Sixuan Wu, Baohong Jiang, Lijun Zeng, Yuanbin Tang, Lunqi Luo, and Lianjie Ouyang assisted in data collection and analysis, as well as in the preparation of cell samples. Wei Du contributed significantly to the pathological analysis and data interpretation. Yuehua Li, played a pivotal role in overseeing the entire project, guiding the research direction, and ensuring the integrity of the work. All authors read and approved the final manuscript.

Funding
This research was funded by the Natural Science Foundation of Hunan Province (2023JJ60495, 2023JJ60496), Clinical Medical Research 4310 Program of the University of South China (20224310NHYCG07) and the Scientific Research Fund Project of Hunan Provincial Health Commission (B202303109577 and D202303109450).

Data availability
The original contributions presented in the study are included in the article/supplementary materials, further inquiries can be directed to the corresponding author/s.

Declaration

Ethics approval and consent to participate
This study involves human tissue samples and animal experiments. All collections of human tissue samples related to this study have been conducted with the patient's informed consent. All procedures of this study have been approved by the Ethics Committee Board of the First Affiliated Hospital of University of South China and were strictly conducted in accordance with the principles of the Declaration of Helsinki. For the animal experiments, we ensured that all experimental animals received proper care and humane treatment. All experimental procedures were conducted with the welfare of the animals in mind, and efforts were made to minimize animal distress.

Consent for publication
Not applicable.

Competing interests
The authors declare no competing interests.

Received: 27 June 2024 / Accepted: 5 September 2024
Published online: 05 October 2024

References

1. Liu H, Dilger JP, Lin J. Lidocaine Suppresses Viability and Migration of Human Breast Cancer Cells: TRPM7 as a Target for Some Breast Cancer Cell Lines. Cancers (Basel). 2021;13(2):234. Published 2021 Jan 10. https://doi.org/10.3390/cancers13020234
2. Lima SM, Kehm RD, Terry MB. Global breast cancer incidence and mortality trends by region, age-groups, and fertility patterns. EClinicalMedicine. 2021;38:100985. https://doi.org/10.1016/j.eclinm.2021.100985. Published 2021 Jul 7.
3. Momenimovahed Z, Salehiniya H. Epidemiological characteristics of and risk factors for breast cancer in the world. Breast Cancer (Dove Med Press). 2019;11:151–64. https://doi.org/10.2147/BCTT.S176070. Published 2019 Apr 10.

4. Youn HJ, Han W. A review of the epidemiology of breast Cancer in Asia: focus on risk factors. Asian Pac J Cancer Prev. 2020;21(4):867–80. https://doi.org/10.31557/APJCP.2020.21.4.867. Published 2020 Apr 1.
5. Yan G, Li Y, Zhan L, et al. Decreased mir-124-3p promoted breast cancer proliferation and metastasis by targeting MGAT5. Am J Cancer Res. 2019;9(3):585–96. Published 2019 Mar 1.
6. Ayama-Canden S, Tondo R, Piñeros L, et al. IGDQ motogenic peptide gradient induces directional cell migration through integrin (αv)β3 activation in MDA-MB-231 metastatic breast cancer cells. Neoplasia. 2022;31:100816. https://doi.org/10.1016/j.neo.2022.100816.
7. Xiang Z, Zhou X, Miranda GM, et al. Identification of the ferroptosis-related ceRNA network related to prognosis and tumor immunity for gastric cancer. Aging. 2022;14(14):5768–82. https://doi.org/10.18632/aging.204176.
8. Ferrand N, Fert A, Morichon R, Radosevic-Robin N, Zaoui M, Sabbah M. WISP2/CCN5 suppresses vasculogenic mimicry through inhibition of YAP/TAZ signaling in breast Cancer cells. Cancers (Basel). 2022;14(6):1487. https://doi.org/10.3390/cancers14061487. Published 2022 Mar 14.
9. Zhao M, Ding N, Wang H, et al. Activation of TRPA1 in bladder Suburothelial myofibroblasts counteracts TGF-β1-Induced Fibrotic Changes. Int J Mol Sci. 2023;24(11):9501. https://doi.org/10.3390/ijms24119501. Published 2023 May 30.
10. Nagaraj G, Ma CX. Clinical challenges in the management of hormone Receptor-Positive, human epidermal growth factor receptor 2-Negative metastatic breast Cancer: a Literature Review. Adv Ther. 2021;38(1):109–36. https://doi.org/10.1007/s12325-020-01552-2.
11. Ji F, Yuan JM, Gao HF, et al. Tumor Microenvironment characterization in breast Cancer identifies prognostic and neoadjuvant chemotherapy relevant signatures. Front Mol Biosci. 2021;8:759495. https://doi.org/10.3389/fmolb.2021.759495. Published 2021 Oct 11.
12. Li X, Ma Z, Mei L. Cuproptosis-related gene SLC31A1 is a potential predictor for diagnosis, prognosis and therapeutic response of breast cancer. Am J Cancer Res. 2022;12(8):3561–80. Published 2022 Aug 15.
13. Munn DH, Bronte V. Immune suppressive mechanisms in the tumor microenvironment. Curr Opin Immunol. 2016;39:1–6. https://doi.org/10.1016/j.coi.2015.10.009.
14. T GS. Innate and adaptive immune cells in Tumor microenvironment. Gulf J Oncolog. 2021;1(35):77–81.
15. Hempelmann P, Lolicato F, Graziadei A, et al. The sterol transporter STARD3 transports sphingosine at ER-lysosome contact sites. Preprint bioRxiv. 2023. https://doi.org/10.1101/2023.09.18.557036. 2023.09.18.557036. Published 2023 Sep 18.
16. Yacov N, Kafri P, Salem Y, et al. MOSPD2 is a therapeutic target for the treatment of CNS inflammation. Clin Exp Immunol. 2020;201(2):105–20. https://doi.org/10.1111/cei.13448.
17. León-Mateos L, Abalo A, Casas H, et al. Global gene expression characterization of circulating Tumor cells in metastasic castration-resistant prostate Cancer patients. J Clin Med. 2020;9(7):2066. https://doi.org/10.3390/jcm9072066. Published 2020 Jul 1.
18. Yu Y, Zhang J, Ni L, et al. Neoantigen-reactive T cells exhibit effective anti-tumor activity against colorectal cancer. Hum Vaccin Immunother. 2022;18(1):1–11. https://doi.org/10.1080/21645515.2021.1891814.
19. Wang Y, Lu G, Xue X, et al. Characterization and validation of a ferroptosis-related LncRNA signature as a novel prognostic model for lung adenocarcinoma in tumor microenvironment. Front Immunol. 2022;13:903758. https://doi.org/10.3389/fimmu.2022.903758. Published 2022 Aug 9.
20. Kulcsar KA, Coleman CM, Beck SE, Frieman MB. Comorbid diabetes results in immune dysregulation and enhanced disease severity following MERS-CoV infection. JCI Insight. 2019;4(20):e131774. https://doi.org/10.1172/jci.insight.131774. Published 2019 Oct 17.
21. de Brito AA, Gonçalves Santos T, Herculano KZ, et al. Photobiomodulation Therapy restores IL-10 secretion in a murine model of Chronic Asthma: relevance to the Population of $CD4^{+}CD25^{+}Foxp3^{+}$ cells in lung. Front Immunol. 2022;12:789426. https://doi.org/10.3389/fimmu.2021.789426. Published 2022 Feb 2.
22. Kirfel J, Kümpers CC, Fähnrich A et al. PD-L1 Dependent Immunogenic Landscape in Hot Lung Adenocarcinomas Identified by Transcriptome Analysis. Cancers (Basel). 2021;13(18):4562. Published 2021 Sep 11. https://doi.org/10.3390/cancers13184562
23. Kutukculer N, Azarsiz E, Aksu G, Karaca NE. CD4 + CD25 + Foxp3 + T regulatory cells, Th1 (CCR5, IL-2, IFN-γ) and Th2 (CCR4, IL-4, Il-13) type chemokine receptors and intracellular cytokines in children with common variable immunodeficiency. Int J Immunopathol Pharmacol. 2016;29(2):241–51. https://doi.org/10.1177/0394632015617064.
24. Horie C, Zhu C, Yamaguchi K, et al. Motile sperm domain containing 1 is upregulated by the Wnt/β-catenin signaling pathway in colorectal cancer. Oncol Lett. 2022;24(2):282. https://doi.org/10.3892/ol.2022.13402. Published 2022 Jun 27.
25. Wang Y, Goliwas KF, Severino PE, et al. Mechanical strain induces phenotypic changes in breast cancer cells and promotes immunosuppression in the tumor microenvironment. Lab Invest. 2020;100(12):1503–16. https://doi.org/10.1038/s41374-020-0452-1.
26. Chen W, Dai X, Chen Y et al. Significance of STAT3 in Immune Infiltration and Drug Response in Cancer. Biomolecules. 2020;10(6):834. Published 2020 May 29. https://doi.org/10.3390/biom10060834
27. Xu W, Ren D, Yu Z, et al. Bacteria-mediated tumor immunotherapy via photothermally-programmed PD1 expression. Nanoscale Adv. 2022;4(6):1577–86. https://doi.org/10.1039/d1na00857a. Published 2022 Feb 7.
28. Zheng Y, Fang YC, Li J. PD-L1 expression levels on tumor cells affect their immunosuppressive activity. Oncol Lett. 2019;18(5):5399–407. https://doi.org/10.3892/ol.2019.10903.
29. Liu T, Cao H, Ji Y et al. Interaction of dendritic cells and T lymphocytes for the therapeutic effect of Dangguiliuhuang decoction to autoimmune diabetes. Sci Rep. 2015;5:13982. Published 2015 Sep 11. https://doi.org/10.1038/srep13982
30. Takashima Y, Kawaguchi A, Kanayama T, Hayano A, Yamanaka R. Correlation between lower balance of Th2 helper T-cells and expression of PD-L1/PD-1 axis genes enables prognostic prediction in patients with glioblastoma. Oncotarget. 2018;9(27):19065–78. https://doi.org/10.18632/oncotarget.24897. Published 2018 Apr 10.
31. Onzi GR, D'Agustini N, Garcia SC, et al. Chemobrain in breast Cancer: mechanisms, clinical manifestations, and potential interventions. Drug Saf. 2022;45(6):601–21. https://doi.org/10.1007/s40264-022-01182-3.
32. Lan YL, Chen C, Wang X, et al. Gamabufotalin induces a negative feedback loop connecting ATP1A3 expression and the AQP4 pathway to promote temozolomide sensitivity in glioblastoma cells by targeting the amino acid Thr794. Cell Prolif. 2020;53(1):e12732. https://doi.org/10.1111/cpr.12732.
33. Kim T, Han S, Chun Y, et al. Comparative characterization of 3D chromatin organization in triple-negative breast cancers. Exp Mol Med. 2022;54(5):585–600. https://doi.org/10.1038/s12276-022-00768-2.
34. Puiffe ML, Le Page C, Filali-Mouhim A, et al. Characterization of ovarian cancer ascites on cell invasion, proliferation, spheroid formation, and gene expression in an in vitro model of epithelial ovarian cancer. Neoplasia. 2007;9(10):820–9. https://doi.org/10.1593/neo.07472.
35. Salem Y, Yacov N, Propheta-Meiran O, Breitbart E, Mendel I. Newly characterized motile sperm domain-containing protein 2 promotes human breast cancer metastasis. Int J Cancer. 2019;144(1):125–35. https://doi.org/10.1002/ijc.31665.
36. Charafe-Jauffret E, Ginestier C, Iovino F, et al. Aldehyde dehydrogenase 1-positive cancer stem cells mediate metastasis and poor clinical outcome in inflammatory breast cancer. Clin Cancer Res. 2010;16(1):45–55. https://doi.org/10.1158/1078-0432.CCR-09-1630.
37. Qi C, Lei L, Hu J, Wang G, Liu J, Ou S. Identification of a five-gene signature deriving from the vacuolar ATPase (V-ATPase) sub-classifies gliomas and decides prognoses and immune microenvironment alterations. Cell Cycle. 2022;21(12):1294–315. https://doi.org/10.1080/15384101.2022.2049157.
38. Chen H, Chong W, Yang X et al. Age-related mutational signature negatively associated with immune activity and survival outcome in triple-negative breast cancer. Oncoimmunology. 2020;9(1):1788252. Published 2020 Jun 30. https://doi.org/10.1080/2162402X.2020.1788252
39. Ozturk E, Catak MC, Kiykim A et al. Clinical and Laboratory Factors Affecting the Prognosis of Severe Combined Immunodeficiency [published correction appears in J Clin Immunol. 2023;43(5):1032. doi: 10.1007/s10875-023-01455-1]. J Clin Immunol. 2022;42(5):1036–1050. https://doi.org/10.1007/s10875-022-01262-0
40. Fan ZY, Han TT, Zuo W, et al. CMV infection combined with acute GVHD associated with poor CD8 + T-cell immune reconstitution and poor prognosis post-HLA-matched allo-HSCT. Clin Exp Immunol. 2022;208(3):332–9. https://doi.org/10.1093/cei/uxac047.
41. Yan Y, Nie K, Zheng J, et al. High endothelin receptor type a expression as an independent Prognostic Biomarker and correlated with Immune infiltrates in stomach adenocarcinoma. Cancer Manag Res. 2021;13:5013–26. https://doi.org/10.2147/CMAR.S313078. Published 2021 Jun 28.

42. Chen Y, Sun J, Luo Y, et al. Pharmaceutical targeting Th2-mediated immunity enhances immunotherapy response in breast cancer. J Transl Med. 2022;20(1):615. https://doi.org/10.1186/s12967-022-03807-8. Published 2022 Dec 23.
43. Formenti SC, Hawtin RE, Dixit N, et al. Baseline T cell dysfunction by single cell network profiling in metastatic breast cancer patients. J Immunother Cancer. 2019;7(1):177. https://doi.org/10.1186/s40425-019-0633-x. Published 2019 Jul 11.
44. Yu J, Wu X, Song J, et al. Loss of MHC-I antigen presentation correlated with immune checkpoint blockade tolerance in MAPK inhibitor-resistant melanoma. Front Pharmacol. 2022;13:928226. https://doi.org/10.3389/fphar.2022.928226. Published 2022 Aug 26.
45. Liu S, Qin T, Liu Z, et al. Anlotinib alters tumor immune microenvironment by downregulating PD-L1 expression on vascular endothelial cells. Cell Death Dis. 2020;11(5):309. https://doi.org/10.1038/s41419-020-2511-3. Published 2020 May 4.
46. Feng Y, Jin H, Guo K, et al. Results from a Meta-analysis of combination of PD-1/PD-L1 and CTLA-4 inhibitors in Malignant Cancer patients: does PD-L1 matter? Front Pharmacol. 2021;12:572845. https://doi.org/10.3389/fphar.2021.572845. Published 2021 Feb 25.

Publisher's note